TRANSPORT PROCESSES IN TEFLON-BONDED FUEL CELL ELECTRODES

By

MYUNG-CHEEN LEE

A DISSERTATION PRESENTED TO THE GRADUATE COUNCIL OF
THE UNIVERSITY OF FLORIDA
IN PARTIAL FULFILLMENT OF THE REQUIREMENTS FOR THE
DEGREE OF DOCTOR OF PHILOSOPHY

UNIVERSITY OF FLORIDA

1976

Dedicated

to my family

ACKNOWLEDGMENTS

The author wishes to express his sincere appreciation to Professor R. D. Walker, Jr., whose invaluable guidance and help made this research project possible and made the author's graduate program a successful experience.

The author is grateful to Drs. D. O. Shah and H. E. Schweyer for serving on the Supervisory Committee and for providing helpful suggestions, and to Drs. Antal Majthay and C. P. Luehr for serving on the Supervisory Committee. He is also indebted to Dr. M. K. Tham for helpful discussions and suggestions.

With deep appreciation the author wishes to thank his mother for her encouragement and his wife, Jungboon, and Mrs. Roswitha Zamorano for typing the manuscript of his dissertation.

The support of this research by the National Aeronautics and Space Administration under Contract NGR 10-005-022 is gratefully acknowledged.

TABLE OF CONTENTS

		Page
ACKNOWLEDGMENTS		iii
LIST OF TABLES		vii
LIST OF FIGURES		viii
KEY TO SYMBOLS		ix
ABSTRACT		xv
CHAPTER		
I	INTRODUCTION	1
	1.1 General Description of Fuel Cell Structure and the Alkaline Hydrogen-Oxygen Fuel Cell	1
	1.2 Thermodynamics and Kinetics of Electrodes	4
	1.3 Advantages of Porous Gas Diffusion Electrodes	11
II	THE STRUCTURE OF TEFLON-BONDED ELECTRODES	13
	2.1 Characterization of Electrode Material	13
	2.2 Surface Area Measurements	14
	2.2.1 Method of Measurements	14
	2.2.2 Experimental Results and Discussion	17
	2.2.3 Estimation of Total and Free Surface Areas of Electrode Components	19
	2.2.4 Estimation of Catalyst Layer Thickness on Teflon Aggregates	21
	2.2.5 Comparison of the Calculated and Measured Surface Areas of 80:20 and 50:50 Pt-black-Teflon Layers and Pure Teflon Layer	23
	2.3 Formation of Electrodes	24
	2.4 Structure of Electrodes	25

TABLE OF CONTENTS (Continued)

CHAPTER		Page
III	ELECTRODE REACTIONS, IONIC HYDRATION, AND WATER TRANSPORT	33
	3.1 Introduction	33
	3.2 Mass Transfer in the Electrolyte Matrix	35
	3.3 Transference Numbers in KOH Solutions	40
	3.4 The Primary Hydration Numbers in Concentrated KOH Solutions	41
	3.5 Concentration Gradients in the Electrolyte Matrix	45
	3.5.1 Concentration Gradients of "Free" Water	45
	3.5.2 Concentration Gradients of KOH Solution	46
	3.6 Discussion	48
IV	MATHEMATICAL MODEL OF TEFLON-CATALYST LAYER AND CALCULATION OF CURRENT DENSITY DISTRIBUTION	50
	4.1 Introduction	50
	4.2 Electrode Reaction and Reaction Rate	56
	4.3 Ionic Fluxes in the Electrolyte Phase	57
	4.4 Potential Gradients in the Electrode Layer	58
	4.5 Oxygen Transport in the Electrolyte Phase	59
	4.6 Computation of the Current Generation	61
	4.7 Results and Discussion	62
V	SUMMARY AND CONCLUSION	69
APPENDIX		
1	DERIVATION OF FLUX EQUATIONS (EQUATIONS (3.3-5) AND (3.3-6))	74
2	DERIVATION OF EQUATION (3.3-10)	78
3	CONVERSION OF D^V TO D*	82

TABLE OF CONTENTS (Continued)

APPENDIX		Page
4	CALCULATION OF C_3 (r,x) FOR A GIVEN x	84
5	COMPUTER PROGRAMMING FOR THE COMPUTATION OF CURRENT DENSITY DISTRIBUTION	88
LIST OF REFERENCES		94
BIOGRAPHICAL SKETCH		96

LIST OF TABLES

Table		Page
2.1	Dependence of Surface Area of Platinum Black on Pretreatment Temperature	17
2.2	Total and Free Surface Areas of Teflon and Pt-black	21
2.3	Calculated and Measured Surface Areas of Pt-black-Teflon Mixtures and Pure Teflon	23
3.1	Summary of Transference Number for KOH Solutions	42
3.2	Concentration of "Free" Water as a Function of Hydration Number	43
3.3	"Free" Water Concentration Gradients	47
3.4	KOH Concentration Gradients in Electrolyte Matrix	49
4.1	Fraction of Current Generation in the Electrode Layer	63
4.2	Cell Potential and Power Density vs. Current Density	66

LIST OF FIGURES

Figure		Page
1.1	Schematic Diagram of an Alkaline Hydrogen-Oxygen Fuel Cell	3
1.2	A Typical Cell Potential-Current Density Relation for a Cell	8
2.1	Dependence of Surface Area of Platinum Black on Pretreatment Temperature	18
2.2	Scanning Electron Micrograph of Pure Teflon Particles. Magnification: 50,000	28
2.3	Scanning Electron Micrograph of Pt-black-Teflon Mixtures. Magnification: 36,000	28
2.4	Scanning Electron Micrograph of Pt-black-Teflon Mixtures. Magnification: 72,000	29
2.5	Scanning Electron Micrograph of a Fuel Cell Electrode. Magnification: 30,000	29
3.1	Concentration of "Free" Water for Different Values of Hydration Number	44
4.1	Scanning Electron Micrograph of the Surface of the 80:20 Pt-black-Teflon Layer. Magnification: 72,000	51
4.2	Schematic Diagram of Platinum Black Catalyst and Teflon Particles in Electrodes	53
4.3	Schematic Model of the Structure of the Catalyst-Teflon Layer	54
4.4	Schematic Model of the Structure of the Catalyst-Teflon Layer with No Windows	55
4.5	Current Generation Distribution in the Electrode Layer	64
4.6	Cumulative Fraction of Current Generation in the Electrode Layer	65
4.7	Cell Potential and Power Density vs. Current Density	67

KEY TO SYMBOLS

a	Activity of KOH electrolyte
A	Onsager equation parameter
B	Onsager equation parameter
C	Constant expressing the net adsorption energy
C	Concentration of KOH, mole/l
C_{fw}	Concentration of free water, mole/l
C_i	Concentration of species i, mole/l
C_O	Concentration of oxidized substance, mole/l
C_R	Concentration of reduced substance, mole/l
C_i^o	Concentration of species i at x = 0, mole/l
C_T	Total solution concentration, mole/l
d	Diameter of particles, cm
d_o	Diameter of adsorbing gas molecule, cm
D*	Diffusivity based on molar average, cm^2/sec
D^v	Diffusivity based on volume average, cm^2/sec
D_i^T	Thermal diffusion coefficient of species i, g/cm-sec
$\mathcal{D}_{ij}$	Diffusion coefficient describing the interaction of species i and j, cm^2/sec
e	Electronic charge, 1.602×10^{-19} Coulomb
E	Internal energy, J/mole
E	Cell potential, volt
E_{oc}	Open circuit cell potential, volt
E_r	Reversible cell potential, volt

E_w	Working cell potential, volt
F	Faraday's constant, 96,487 Coulomb/equiv.
G	Free energy, J/mole
H	Enthalpy, J/mole
i	Current density, amp/cm^2
i_o	Exchange current density, amp/cm^2
i_{lim}	Limiting current density, amp/cm^2
i_s	Catalyst phase current density, amp/cm^2
i_ℓ	Electrolyte phase current density, amp/cm^2
j_i	Mass flux of species i, mole/cm^2/sec
k	Rate constant
k	Conductivity of electrolyte, mho/cm
k_1	Slope of BET plot
k_2	Intercept of BET plot
k_f	Rate constant of forward reactions
k_r	Rate constant of reverse reactions
k^o	Rate constant in the absence of a potential difference
L	Thickness of electrode layer, cm
M_i	Molecular weight of species i, g/mole
m	Molality of electrolyte, mole/kg
n	Number of electrons transferred in electrochemical reactions
N_i	Molar flux of species i
P	Partial pressure of adsorbing gas, mmHg
P	Pressure of the system, atm
P_o	Saturation pressure of nitrogen at -195°C, 780 mmHg
Q	Heat adsorbed by the system, J/mole
r	Radial position coordinate, cm

r_o	Average radius of Teflon aggregates, cm
R	Gas constant, 8.314 joule/mole/°K
R_e	External resistance, ohm
R_i	Internal resistance, ohm
s	Primary hydration number
s_i	Stoichiometric number of species i
$\bar{s}_i$	Partial entropy of species i, J/mole-deg
S	Entropy of the system, Cal/mole-deg
t_i	transference number of species i
T	Temperature of the system, °K
v	Reaction velocity
v_i	Velocity of species i
v_o	Velocity of solvent
V	Volume of the system, cm^3
V_a	Potential of the anode, volt
V_{ads}	Total volume of adsorbed gas on the surface of the adsorbent, ml
V_c	Potential at the cathode, volt
V_m	Volume of adsorbed gas when the entire adsorbent surface is covered with a mono molecular layer, ml
$V_{r,a}$	Reversible potential at the anode, volt
$V_{r,c}$	Reversible potential at the cathode, volt
$\bar{V}_i$	Partial molar volume of species i, l/mole
W	Work involved in the operation of a cell, J/mole
W_{el}	Electrical work in the operation of a cell, J/mole
W'_{el}	Electrical work that can be done per act of an overall reaction, J/mole
x	Axial position coordinate, cm
z_i	Charge number of species i

Greek letters

α_a	Transfer coefficient at the anode
α_c	Transfer coefficient at the cathode
β	Symmetry factor
γ	Activity coefficient
δ	Thickness of electrolyte-catalyst phase, cm
ε	Porosity
κ	Conductivity of electrolyte, mho/cm
ρ	Density of electrolyte, g/cm^3
ϕ_ℓ	Potential in the electrolyte phase, volt
ϕ_s	Potential in the catalyst phase, volt
ξ	Transfer coefficient
η_a	Sum of overpotentials at the anode, volt
η_c	Sum of overpotentials at the cathode, volt
η_{ohm}	Ohmic potential loss, volt
λ_i	Equivalent conductance of species i, $mho\text{-}cm^2/equiv.$
λ_i^o	Equivalent conductance of species i at infinite dilution
μ	Electrochemical potential of species i, J/mole
ν	Total number of ions produced by the dissociation of one molecule of electrolyte
ν_i	Number of ions of species i produced by the dissociation of one molecule of electrolyte
σ	Conductivity of catalyst phase, mho/cm

Subscripts

a	Anode
A	Major
act	Activation
ads	Adsorbed

B	Minor
c	Cathode
conc	Concentration
e	Electrical
e	External
f	Forward
fw	Free water
i	Internal
i	Species i
j	Species j
ℓ	Electrolyte phase
m	Monolayer
O	Oxidized material
oc	Open circuit
r	Reverse
r	Reversible
R	Reduced material
s	Catalyst phase
T	Total
w	Working
x	x-direction
1	Hydroxyl ion
2	Potassium ion
3	Oxygen
4	Water
+	Positive ion
-	Negative ion

Superscripts

0	Initial value at x=0
*	Molar average
v	Volume average
T	Thermal

Abstract of Dissertation Presented to the Graduate Council
f the University of Florida in Partial Fulfillment of the Requirements
for the Degree of Doctor of Philosophy

TRANSPORT PROCESSES IN TEFLON-BONDED FUEL CELL ELECTRODES

By

Myung-Cheen Lee

December, 1976

Chairman: Robert D. Walker, Jr.
Major Department: Chemical Engineering

The structure and properties of Teflon-bonded fuel cell electrodes and their components--platinum black and Teflon 30 particles--has been investigated in detail and compared with previously published works. Recent experiments employing scanning electron microscopy and energy dispersive X-ray analysis indicate that the Teflon particles are prolate spheroidal aggregates of approximately spherical Teflon molecules. In a commonly used electrode composition these Teflon aggregates are coated with one or more layers of catalyst crystallites. The dimensions of the Teflon aggregates are approximately 1500 x 3000 A, the diameter of the Teflon molecules ranges from 200 to about 300 A, while the diameter of the catalyst crystallites appears to be 30 to 40 A.

Electrode reactions, ionic hydration, water transport, and their effects on the behavior of fuel cells have been studied. These studies suggest that hydration of potassium and hydroxyl ions, which has been ignored in previous studies,

causes some change in the concentration of electrolyte and its gradient in the electrolyte matrix and the electrode layer.

On the basis of the new knowledge of the electrode structure, the properties of its components, and its geometry a mathematical model has been developed to enable one to predict the current distribution in the electrode layer. These calculations show, as one might expect, that at high current densities the great majority of the current is generated in a very thin layer of the Teflon-bonded catalyst immediately adjacent to the electrolyte matrix. For an oxygen electrode operating at a current density of one ampere per cm^2 more than half of the current is generated in the 20 % of the catalyst-Teflon layer nearest the electrolyte matrix. At low current densities current generation is relatively uniform throughout this layer.

CHAPTER I

INTRODUCTION

1.1 General Description of Fuel Cell Structure and the Alkaline Hydrogen-Oxygen Fuel Cell

A fuel cell is a direct energy conversion device generating electricity by oxidation of a fuel at one electrode and reduction of an oxidant at another electrode. Thus, chemical energy is converted directly into electrical energy, by which method the fundamental limitation of the Carnot cycle is avoided. In principle, therefore, higher efficiencies can be attained in fuel cells than those attained in heat engines. Hydrogen, hydrocarbons, and other compounds can be used as fuels while oxygen is most frequently used as the oxidant either pure or as air.

Among the various kinds of fuel cells which have been developed, the hydrogen-oxygen system in alkaline electrolyte is probably the most advanced and widely used. However, its technology has far outpaced our understanding of its behavior and operative mechanisms.

Since gaseous hydrogen and oxygen are used as fuel and oxidant, gas diffusion electrodes are used for both anode and cathode. The electrodes are usually made by

depositing a mixture of catalyst and binder on a wire screen which serves both as an electron collector and a mechanical support. If Teflon is used as the binder, it can confer a degree of hydrophobicity to the electrodes which makes it possible for gaseous reactants to diffuse readily to reaction sites. Between the anode and the cathode there is an electrolyte matrix which provides electrical insulation between the electrodes as well as a porous medium through which diffusion and migration can occur under the influence of concentration and potential gradients. An electrolyte reservoir is also used to hold extra electrolyte and to assist in evaporation of water produced by the overall cell reaction; it is usually a sintered metal plate. A schematic diagram of a fuel cell is shown in Figure 1.1.

The electrochemical reactions occurring in this fuel cell are usually written as follows:

Anode : $2\ H_2 + 4\ OH^- = 4\ H_2O + 4\ e$

Cathode : $O_2 + 2\ H_2O + 4\ e = 4\ OH^-$

Overall Cell Reaction : $2\ H_2 + O_2 = 2\ H_2O$

However, the ions are hydrated and the actual reactions should be written as follows:

Anode : $2\ H_2 + 4[OH^- \cdot sH_2O] = 4(1+s)\ H_2O + 4\ e$

Cathode : $O_2 + 2(1+2s)\ H_2O + 4\ e = 4[OH^- \cdot sH_2O]$

Overall Cell Reaction : $2\ H_2 + O_2 = 2\ H_2O$

where s = the hydration number of the hydroxyl ion.

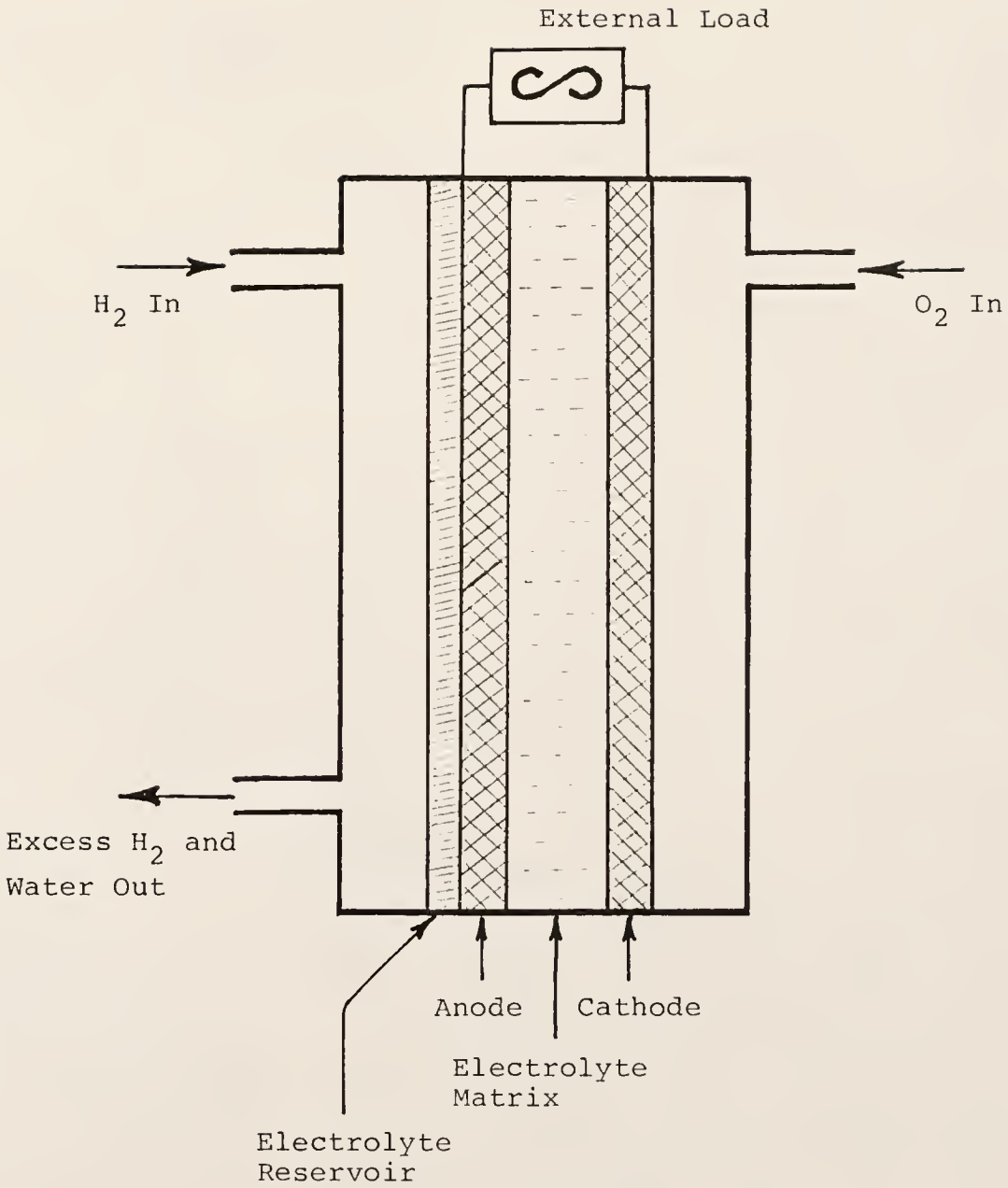

Figure 1.1: Schematic Diagram of an Alkaline H_2-O_2 Fuel Cell.

Since water is produced at the anode and consumed at the cathode, both in the formation of hydroxyl ions and in their hydration, water should diffuse from the anode to the cathode, while the hydrated hydroxyl ions should migrate and diffuse from the cathode to the anode. The product water must be removed from the cell to prevent electrolyte dilution. This implies more complicated transport processes than the case when there is no hydration of hydroxyl ions.

1.2 Thermodynamics and Kinetics of Electrodes

When a chemical reaction is carried out electrochemically, the work done, W, is given by

$$\Delta H = \Delta E + P\,\Delta V$$
$$= Q - W + P\,\Delta V \qquad (1.2\text{-}1)$$

where ΔH = enthalpy change of the system, Joule/mole;

ΔE = internal energy change of the system, Joule/mole;

P = pressure of the system, atm;

ΔV = volume change of the system, cm^3;

Q = heat absorbed by the system, Joule/mole.

W is not only the work of expansion done by gases produced, but also the electrical work involved in transporting electric charge around the external circuit from the anode to the cathode at which the potentials are $V_{r,a}$ and $V_{r,c}$, respectively. The maximum electrical work that can be done

per act of an overall reaction, W', carried out in a cell and which involves transfer of n electrons is

$$W'_{el} = n\ e\ (V_{r,c} - V_{r,a}) \qquad (1.2\text{-}2)$$

for a hypothetical case in which the internal resistance of the cell and overpotential losses are negligible. Conversion to a molar basis by multiplying by Avogadro's number gives

$$W_{el} = n\ F\ (V_{r,c} - V_{r,a}) \qquad (1.2\text{-}3)$$

where F = Faraday's constant, equal to 96,487 coulombs/equivalent.

Since the only forms of work involved in the operation of the electrochemical cell are electrical work and work of expansion,

$$W = W_{el} + P\ \Delta V \qquad (1.2\text{-}4)$$

If, in addition, the process is carried out reversibly,

$$Q = T\ \Delta S \qquad (1.2\text{-}5)$$

where ΔS = entropy change of the system, Joule/mole-°K;

T = temperature of the system, °K.

Using Equations (1.2-1), (1.2-3), (1.2-4), and (1.2-5), it follows that

$$\Delta H = T\ \Delta S - n\ F\ (V_{r,c} - V_{r,a}) \qquad (1.2\text{-}6)$$

By comparison of Equation (1.2-6) with

$$\Delta G = \Delta H - T\,\Delta S \qquad (1.2\text{-}7)$$

where ΔG = free energy change of the system, which holds for an isothermal process, we get

$$\Delta G = -n\,F\,(V_{r,c} - V_{r,c}) \qquad (1.2\text{-}8)$$

Writing $V_{r,c} - V_{r,a} = E_r$, we get

$$\Delta G = -n\,F\,E_r \qquad (1.2\text{-}9)$$

where E_r is the electromotive force of the reversible cell. Thus, an ideal fuel cell yields electrical energy equivalent to the free energy change of the reaction.

In the normal operation of a fuel cell, the electrical energy must be supplied at a significant rate, and under these conditions reversibility cannot be maintained. In practice, the cell potential, E, of an electrochemical device working at an appreciable rate (current) is given by

$$E = E_r - \Sigma\eta \qquad (1.2\text{-}10)$$

where $\Sigma\eta$ is the sum of all of the overpotentials that exist at the electrodes, electrode-electrolyte interfaces, and ohmic losses in the electrolyte. The factors that affect the working voltage of a cell are the activation overpotential, ohmic losses, and mass transfer (concentration) overpotential. The activation overpotential results from the slowness of one or more of the reaction steps in either one or both of the electrode reactions. A typical plot of

terminal cell voltage E vs. current density, i, of an operating fuel cell is shown in Figure 2. The open-circuit voltage E_{oc} is often (usually for fuel cells) less than thermodynamically reversible potential E_r, because of the interference caused by possible reactions due to impurities. The effects of impurities generally decrease as the current density increases. It is always found that there is a sharp initial decrease of the working potential E with i, as shown by section AB of the curve in Figure 1.2. This type of behavior is characteristic of highly irreversible processes and is attributed to activation overpotential.

The linear portion BC in Figure 2 corresponds to a relatively high current density region in which the decrease in cell potential with increase of current density is due principally to ohmic losses in the electrolyte. When porous electrodes are used, not only the layer of electrolyte in the electrolyte matrix but also the electrolyte within the pores contributes to the electrolyte resistance.

At sufficient high current densities (i.e., high local reaction rates), most heterogeneous reactions pass into a region where the rate is controlled by the rate of transport of reactants to, or products from, the electrodes. Region CD in Figure 1.2 illustrates this effect, which is known as the concentration (or mass transfer) overpotential.

In the actual operation of fuel cell, the current I, after considering the overpotentials, is given by

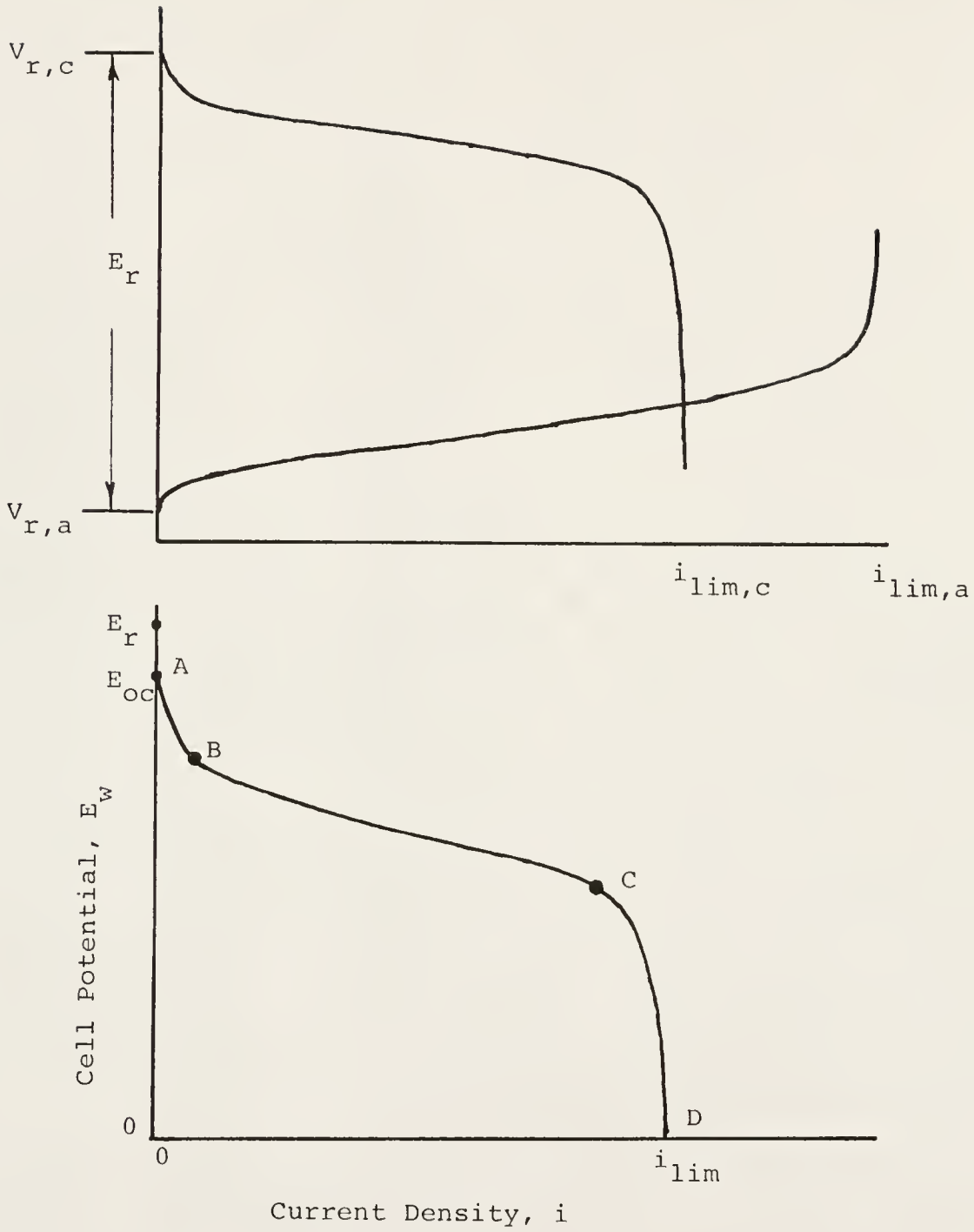

Figure 1.2: A Typical Cell Potential-Current Density Relation for a Cell.

$$I = \frac{(V_c - V_a) - \eta_{ohm}}{R_e} \qquad (1.2\text{-}11)$$

where η_{ohm} = ohmic voltage loss, volt;

R_e = resistance of the external load, ohm;

V_c and V_a = electrode potentials at the cathode and the anode, respectively, which are given by

$$V_c = V_{r,c} - \Sigma\eta_c$$

$$= V_{r,c} - \eta_{c,act} - \eta_{c,conc} \qquad (1.2\text{-}12)$$

$$V_a = V_{r,a} + \Sigma\eta_a$$

$$= V_{r,a} + \eta_{a,act} + \eta_{a,conc} \qquad (1.2\text{-}13)$$

where the suffixes "act" and "conc" denote activation and concentration overpotentials, respectively.

In many electrochemical reactions, the current at a particular electrode is found to vary exponentially with potential across the metal-solution interface, and the relationship between potential and the rate constant k of an electrochemical reaction can be expressed empirically by

$$k = k^o \exp(-\beta VF/RT) \qquad (1.2\text{-}14)$$

where k^o = rate constant in the absence of a potential difference

β = a symmetry factor, $0 \leq \beta \leq 1$

R = gas constant, 8.314 Joule/gmole-°K

The reaction velocity in electrochemical kinetics is related to the current density, i, which is the current per

unit area of electrode surface. The relation between reaction velocity, v, and current density, i, depends on the number of electrons transferred in one act of the overall reaction, n.

$$i = n F v \tag{1.2-15}$$

The rates of electrochemical reactions are a measure of the net reaction rates and the net current density is given by

$$i = \vec{i} - \overleftarrow{i} \tag{1.2-16}$$

where $\vec{i}$ is the forward current and $\overleftarrow{i}$ is the reverse current. Therefore, in the case of the electrode reaction $O + e \rightarrow R$, the net current density may be expressed by (since n = 1)

$$i = F\left[k_f^o C_O \exp\left(-\frac{\beta VF}{RT}\right) - k_r^o C_R \exp\left((1-\beta)\frac{VF}{RT}\right)\right] \tag{1.2-17}$$

where k_f^o and k_r^o are the rate constants of the forward and reverse reactions in the absence of a metal-solution potential difference and C_O and C_R are the concentrations of the oxidized and reduced species, respectively. The exchange current density is related to the velocity, in amp/cm^2, of the forward or backward reaction at equilibrium, in which condition the net current density is zero and the exchange current density i_o is given by

$$\begin{aligned} i_o &= F k_f^o C_O \exp\left(-\frac{\beta VF}{RT}\right) \\ &= F k_r^o C_R \exp\left((1-\beta)\frac{VF}{RT}\right) \end{aligned} \tag{1.2-18}$$

Using Equation (1.2-18) and the overpotential, which is equal to the potential difference $V - V_r$, Equation (1.2-17) can be expressed as

$$i = i_o\left[\exp\left(-\frac{\beta\eta F}{RT}\right) - \exp\,(1-\beta)\,\frac{\eta F}{RT}\right] \qquad (1.2\text{-}19)$$

In the case of a multielectron transfer reaction, the general form of the current density-overpotential relation is

$$i = i_o\left[\exp\left(-\frac{\alpha_a \eta F}{RT}\right) - \exp\left(\frac{\alpha_c \eta F}{RT}\right)\right] \qquad (1.2\text{-}20)$$

where α_a and α_c are the transfer coefficients of the reactions of the anode and the cathode, respectively, and depend on the mechanism of the overall reaction. In the study of mathematical formulation and solution of electrode models, this equation is most important.

1.3 Advantages of Porous Gas Diffusion Electrodes

For an electrochemical energy conversion system to be useful for practical applications it should be able to provide good power density. Because of the need to minimize the activation overpotential at desired currents, to facilitate mass transfer to the reaction sites, and because both the fuel and the oxidant in hydrogen-oxygen fuel cells are gaseous, porous gas diffusion electrodes are used. The much greater power densities afforded by porous electrodes as compared to planar electrodes is due not only to their high

rates of real to apparent area (i.e., much larger concentrations of reaction sites are available), but also to the fact that they permit much higher limiting currents. Another advantage of porous electrodes is that the catalyst, in the form of very fine particles, can be dispersed within the pores, thereby reducing considerably the quantity of catalyst used.

The difficulty of understanding the behavior and mechanisms of electrode reactions in porous electrodes arises mainly from their extremely complex physical structure and the consequent difficulty of describing them geometrically so that mathematical analysis can be carried out. One of the principal purposes of this study is to examine the detailed structure of Teflon-bonded fuel cell electrodes and to relate this structure to their performance and transport processes, etc., so that we can use the information in understanding and evaluating the behavior and mechanisms of performing electrodes and in designing electrodes capable of improved performance.

CHAPTER II

THE STRUCTURE OF TEFLON-BONDED ELECTRODES

2.1 Characterization of Electrode Material

Teflon-bonded fuel cell electrodes are made of three different materials; catalyst, Teflon, and fine-meshed metal screen. In many cases platinum black is used as the catalyst because of its excellent catalytic properties, i.e., its high exchange current density in alkaline electrolyte. It is a very fine black powder; the crystallite size is so small that individual crystallites have not yet been clearly resolved by scanning electron microscopy, i.e., the crystallite diameter is less than 10 nm (=100 A). However, by surface area measurements using the BET gas adsorption method [1], the average crystallite diameter of a widely used platinum black (Englehard fuel cell grade) is calculated to be about 40 ± 10 A. In its as-received state, the catalyst exists as agglomerates of 1 micron in diameter.

Teflon 30, an aqueous emulsion (DuPont), is usually used for the Teflon component of electrodes. It is a negatively charged hydrophobic colloid containing polytetrafluoroethylene (PTFE) resin particles, 0.05 to 0.5 micron in diameter, suspended in water and stabilized with Triton X-100, a nonionic surfactant. Teflon is very hydrophobic

and is relatively stable up to temperatures of about 350°C. Electron microscopic examination of well-dispersed pure Teflon particles reveals that although the size varies from 500 to 5000 A in diameter, the majority of particles are prolate spheroid in shape, the minor and major diameters being about 1000 to 1500 A and 2000 to 3000 A, respectively. It is also noted that a single Teflon particle appears to be an aggregate of small spherical particles (200 to 300 A in diameter) which may be Teflon molecules. Teflon 30 is reported by the manufacturer to have a mean molecular weight of 5 MM, and calculation suggests that a molecule of this molecular weight should have a diameter of about 200 A. Several scanning electron micrographs of well-dispersed Teflon particles are shown later on pages 28-29.

The fine-meshed metal screen is used to provide mechanical support for the catalyst layer and to serve as an electron collector for the electrons generated. Gold-plated nickel screen about 100 mesh is used for most alkaline fuel cells.

2.2 Surface Area Measurements

2.2.1 Method of Measurements

The surface areas of platinum catalyst, pure Teflon, and electrodes were measured by BET method. This method involves measuring the amount of gas adsorbed on a solid surface at a temperature close to the boiling point of the gas. A quantity of sample is weighed into a sample cell

and pretreated for about 15 hours at 200-220°C while a stream of pure helium flows through the cell to remove moisture and adsorbed species. After the measurement the sample is reweighed to determine the dry weight.

In the continuous flow method developed by Nelsen and Eggertsen [2] nitrogen is used as the adsorbate and helium is used as the carrier gas. A mixture of nitrogen and helium of known composition is passed through the sample and the effluent composition is monitored by thermal conductivity measurements. When the sample is cooled in liquid nitrogen, the adsorption of nitrogen is indicated by a peak on a recorder chart. After adsorption equilibrium is established, the recorder pen returns to its original baseline. The sample tube is allowed to warm by removing the liquid nitrogen coolant, causing desorption of nitrogen and producing a peak on the chart which is in the reverse direction of the adsorption peak.

The area under the desorption peak is a measure of the nitrogen adsorbed. This peak area was calibrated by injecting a known amount of nitrogen into the nitrogen-helium stream to give a peak of similar magnitude to the area of the desorption peak. The amount of nitrogen adsorbed is calculated by comparing these two peak areas. Adsorption, desorption, and calibration are done at several relative nitrogen pressure ratios in the range from 0.05 to 0.3.

After computing the amount of nitrogen adsorbed and the corresponding relative pressures, the amount of nitrogen adsorbed in a monolayer, V_m, is determined from the BET equation:

$$\frac{P}{V_{ads}\ (P_o - P)} = \frac{C - 1}{V_m\ C}\ \frac{P}{P_o} + \frac{1}{V_m\ C} \qquad (2.2\text{-}1)$$

where P = partial pressure of the adsorption gas, mmHg;

P_o = saturation pressure of the adsorption gas over the solid sample at the temperature of coolant, mmHg;

V_{ads} = total volume (STP) of adsorbed gas on the surface of the adsorbent, ml;

C = constant expressing the net adsorption energy;

V_m = volume (STP) of adsorbed gas when the entire adsorbent surface is covered with a monomolecular layer, ml.

When the left hand side of the equation is plotted as the ordinate versus the relative pressure, P/P_o, a straight line with slope $(C - 1)/V_m\ C$ and intercept $1/V_m\ C$ is obtained. If we note that

$$\frac{1}{\text{Slope} + \text{Intercept}} = \frac{1}{\frac{C - 1}{V_m\ C} + \frac{1}{V_m\ C}} = V_m\ , \qquad (2.2\text{-}2)$$

then we can determine V_m from

$$V_m = \frac{1}{k_1 + k_2} \qquad (2.2\text{-}3)$$

where k_1 is the slope and k_2 is the intercept of the straight line. This value, multiplied by the proper factor for the area covered per unit amount of nitrogen, gives the surface area, and when divided by the dry weight of the sample, it yields the specific surface area.

2.2.2 Experimental Results and Discussion

Weighed samples of platinum catalyst (Englehard fuel cell grade platinum black) were heated in a stream of flowing helium for about 15 hours at temperatures ranging from 100 to 400 °C. Then the surface area was measured as described in Section 2.2.1. Since it is standard procedure to sinter fuel cell electrodes fabricated with Teflon-platinum catalyst mixtures at a temperature between 310 and 320 °C, the surface area in the temperature range 300-350 °C was studied carefully. The data are shown in Table 2.1 and in Figure 2.1

Table 2.1

Dependence of Surface Area of Platinum Black on Pretreatment Temperature.

Temp. of Pretreatment, °C	Surface Area, m^2/g
100	45.3
150	46.0
200	48.9
250	49.6
300	48.1
310	44.2
320	37.8
330	12.1
350	5.25
400	5.01

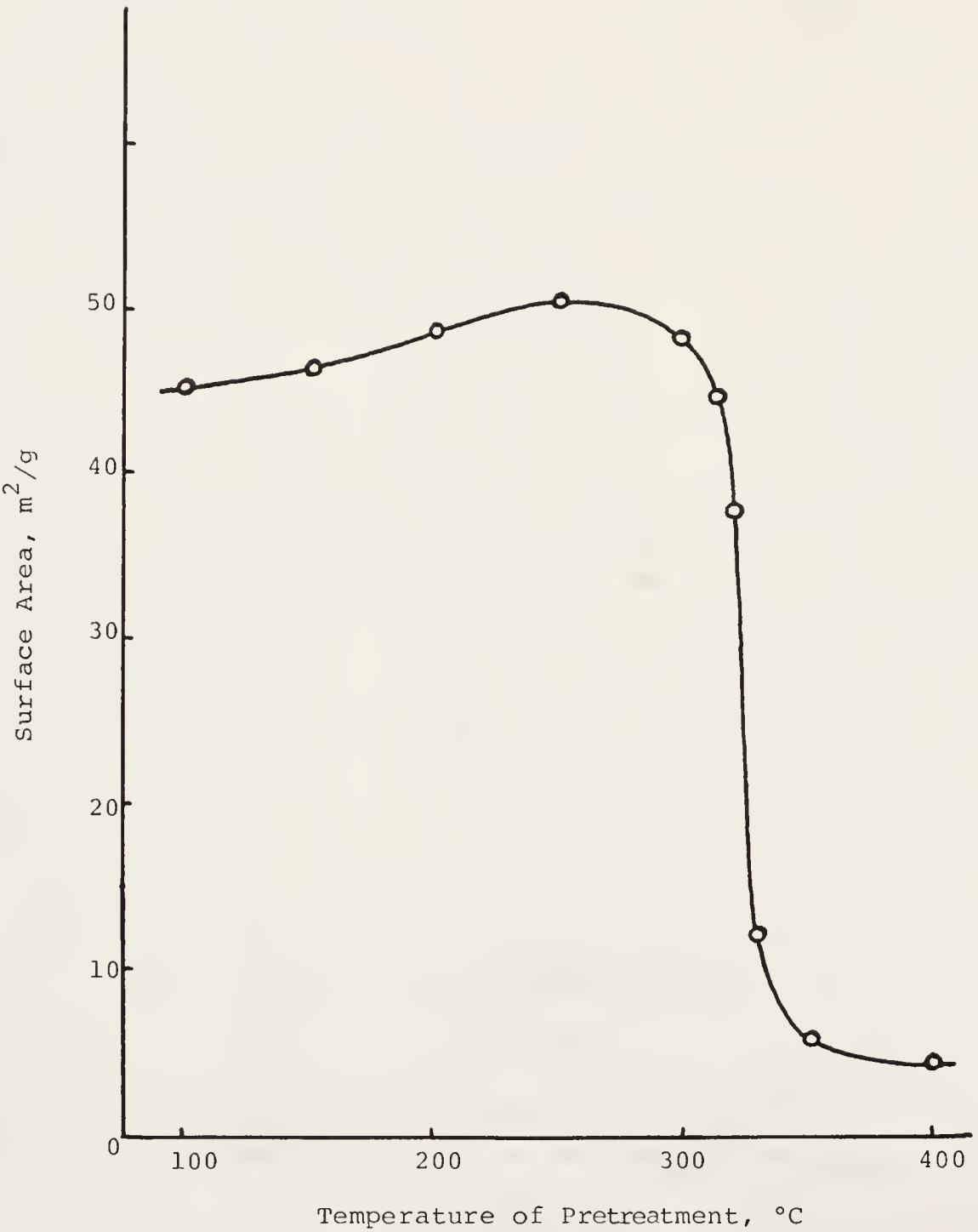

Figure 2.1: Dependence of Surface Area of Pt-black on Pretreatment Temperature.

It is clear that a large decrease in surface area occurred when the pretreating temperature was between 300 and 350 °C. There is a gradual increase in the surface area as the pretreating temperature is increased to 200 °C, but the slight changes in surface area between 200 and 300 °C are probably not significant. However, the reduction of surface area seems to have already begun at 300 °C, and the advantages of sintering the Teflon at 310 - 320 °C must be weighed against the loss in surface area. On the other hand the surface area lost on sintering may be lost fairly early during the life of an electrode, and it may not be significant for the entire life of a fuel cell.

2.2.3 Estimation of Total and Free Surface Areas of Electrode Components

The surface areas of platinum black catalysts and Teflon particles can be estimated by calculation from the information obtained on their sizes. Assuming that both catalyst crystallites and Teflon molecules are spherical and their surfaces smooth, we can calculate the surface areas from

$$S_t = \text{(Surface Area of a Single Particle) X (Number of Particles in 1 gram)}$$

$$= \pi d^2 \times \left(1/\frac{\pi}{6} d^3 \rho\right)$$

$$= 6/\rho d \qquad (2.2\text{-}4)$$

where S_t = total geometrical surface area per one gram, cm^2/g;

ρ = density of the component, g/cm^3;

d = diameter of the component, cm.

In comparing the calculated surface areas with those measured by the BET method the exclusion of surface area due to the presence of neighboring particles should be considered. The fraction of excluded surface area can be estimated from the following [3]:

$$f = \frac{n\, d_o}{2\,(d_o + d)} \qquad (2.2\text{-}5)$$

where f = fraction of excluded surface area;

n = coordination number, i.e., number of contacts per particle;

d_o = diameter of adsorbate gas used in the BET method, cm;

d = diameter of particle, cm.

Therefore, by using Equations (2.2-4) and (2.2-5) and noting that the specific gravity of Teflon is 2.22 and that of platinum is 21.45 while letting the molecular diameter of Teflon and Pt-black range from 200 to 300 A and 10 to 60 A, respectively, d_o = 4.5 A for nitrogen, and n = 4, 6 and 8, we get the results shown in Table 2.2.

Comparing the results with the surface area of platinum black experimentally measured, 45 m^2/g, we can estimate that, assuming the packing condition of platinum black to be random to random-close, the average size of a single catalyst crystallite ranges from 45 to 50 A in diameter. Considering the assumption that the crystallites are uniform smooth spheres, we can see that the actual size of a crystallite can be smaller than what has been estimated, i.e., ranging from 30 to 40 A in diameter.

Table 2.2

Total and Free Surface Areas of Teflon and Pt-black.

	Diameter, A	Calculated Geometric Surface Area, m^2/g	Free Surface Areas, m^2/g n = 4	n = 6	n = 8
	200	135	129	126	123
Teflon	250	108	104	102	100
	300	90	87	86	85
	10	279	106	19	
	20	140	89	63	37.1 (25) 43.7
Platinum Black	30	93	69	57	44.5 (35) 43.5
	40	70	56	49	41.7
	50	56	47	42	37.5
	60	47	40	37	33.9

2.2.4 Estimation of Catalyst Layer Thickness on Teflon Aggregates

In order to be able to estimate the thickness of Pt-black layer on Teflon aggregates it is necessary to know the surface area of Teflon aggregates and the packing condition of Pt-black crystallites on the surface of Teflon aggregates. From the information on the size and the shape of Teflon aggregates we can calculate the surface area of Teflon aggregates as follows:

Surface Area of 1 g of Teflon = (Surface Area of a Teflon Aggregate) X (Number of Aggregates in 1 g of Teflon)

$$= \left[\frac{\pi r}{2}\left(d_B + \frac{d_A d_B}{e}\sin e\right)\right] \times \left[\frac{1}{\frac{\pi}{6} d_A d_B \rho (1-\varepsilon)}\right] \qquad (2.2\text{-}6)$$

where d_A = major diameter of a Teflon aggregate, cm;

d_B = minor diameter of a Teflon aggregate, cm;

e = eccentricity, $e = \sqrt{d_A^2 - d_B^2} / d_A$;

r = roughness factor;

ε = porosity.

Therefore, substituting d_A = 2500 A, d_B = 1250 A, r = 1.5, ε = 0.36 (for random-close packing), and ρ = 2.22, we get the external surface area of Teflon aggregates as 43.3 m^2/g.

The thickness of Pt-black catalyst layer in the mixtures of Pt-black and Teflon can be calculated as follows:

Thickness = (Bulk Volume of Pt-black in 1 g of Mixture)/ (Teflon Aggregate Surface Area in 1 g of Mixture)

$$= \frac{1-x}{\rho(1-\varepsilon)} / (\text{Surface Area of 1 g of Teflon Aggregates x } x) \qquad (2.2\text{-}7)$$

where x = fraction of Teflon in a mixture;

ρ = density of Pt-black crystallites, g/cm^3;

ε = porosity of Pt-black catalyst layer.

Therefore, with an assumption that the packing of Pt-black crystallites on Teflon aggregates' surface is random, which has the porosity of 0.36 to 0.40, we can estimate that an 80:20 Pt-black-Teflon mixture has a catalyst layer thickness

of 70 A and a 50:50 mixture has a catalyst layer thickness of 17 A. Considering the fact that the crystallite size of Pt-black has been estimated to be 30 to 40 A in diameter, we can see that in the 50:50 mixture a fairly significant fraction of the surface of Teflon aggregates is not coated with Pt-black catalyst, although there can still be continuous catalyst connection due to the tendency of catalyst particles collecting in the crevices first.

2.2.5 Comparison of the Calculated and Measured Surface Areas of 80:20 and 50:50 Pt-black-Teflon Layers and Pure Teflon Layer

If we assume that the surface areas of the components of Pt-black-Teflon layers do not change during the formation of electrodes, we can estimate the surface areas of Pt-black-Teflon mixture layers of different ratios from calculations by using pure component surface areas. Comparison of these calculated surface areas with the measured ones is shown in Table 2.3.

Table 2.3

Calculated and Measured Surface Areas of Pt-black-Teflon Mixtures and Pure Teflon.

Pt-black:Teflon wt. % ratio	Calculated Surface Area, m^2/g	Measured Surface Area, m^2/g
80:20	57 (38)	22.0 ± 0.5
50:50	74 (27)	19.0 ± 0.5
Pure Teflon	103	9.5 ± 0.3

As we can see in the results shown above, there is a significant difference between the calculated and the measured surface areas of pure Teflon. Since the pure Teflon sample was prepared by filtration, pressing, and sintering for the measurement of its surface area, there must have occurred a considerable reduction of its surface area during these processing, particularly due to the sintering at 310°C which would cause softening and binding of Teflon aggregates.

If we use the measured surface area of Teflon, 9.5 ± 0.3 m^2/g, in calculating the surface area of the mixtures, we obtain the results shown in the parenthesis in Table 2.3. Comparing these results with the measured surface areas of the Pt-black-Teflon layers of different ratios, we can still notice considerable differences between the calculated and measured surface areas. This can also be attributed to the softening and bonding of Teflon aggregates during sintering, which can cause some portion of Pt-black to be buried in them. This can be shown by the fact that the calculated surface area of Pt-black from the measured surface areas of 80:20 and 50:50 mixtures and pure Teflon is about 27 m^2/g, which would mean that there was a loss about 40 % in the surface area of Pt-black.

2.3 Formation of Electrodes

Fuel cell electrodes can be made in several ways; one method, based on information derived from reports and technical personnel at NASA Laboratories is as follows:

Platinum black is weighted out and dispersed for several minutes in water containing a wetting agent, Triton X-100, in an amount equal to 6% of the weight of catalyst using an ultrasonic agitator. The requisite amount of Teflon 30 emulsion is added to Pt-black dispersion and the ultrasonic agitation is repeated for an additional several minutes. The mixture is filtered on a very fine pore filter. After the catalyst mixture is partially dried at room temperature, a fine-meshed metal screen is placed on the catalyst layer, followed by laying a filter paper on the screen to absorb water and the "sandwich" is pressed at about 5000 psi. The filter papers are then peeled off, and the electrode is sintered in air at 310 °C for about 20 minutes.

2.4 Structure of Electrodes

In understanding various phenomena occurring in an operating fuel cell, it is essential to know the structure of the catalyst layer as this has a great influence on the performance of the cell. Since the catalyst layer of an electrode consists of a mixture of very small hydrophylic Pt-black particles and hydrophobic Teflon particles, their arrangement in the layer will have a great influence on the wettability of electrodes, thereby influencing the transport processes within electrodes. The relative amounts of electrode components, as well as their arrangement, will have influence on these characteristics.

Most of the published work on the structure of Teflon-bonded fuel cell electrodes [4,5] is based on the view that the basic structure of the catalyst layer is one of fairly large catalyst aggregates more or less surrounded by Teflon-particles, the two materials existing as interpenetrating lattices which provide continuous transport paths for both liquid and gas. This view is illustrated in the schematic diagram below.

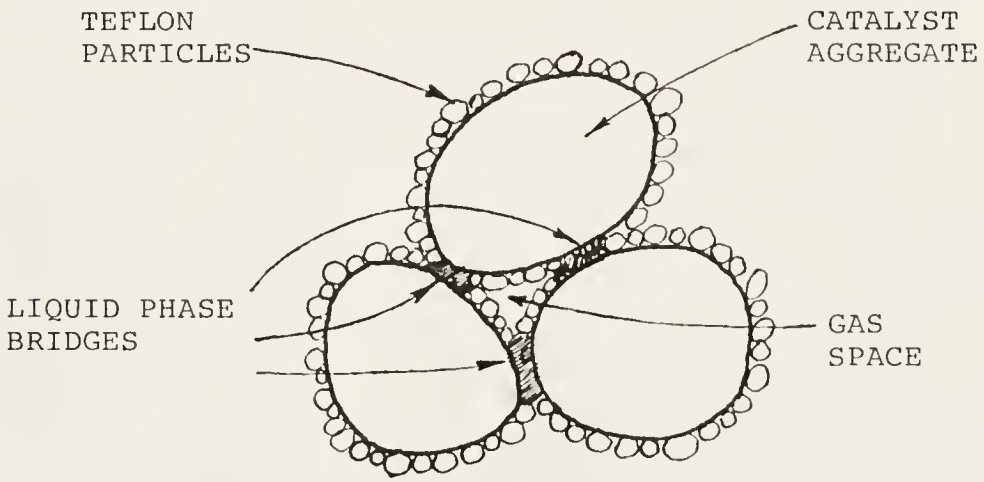

Our recent experiments employing scanning electron microscopy and energy dispersive X-ray analysis have raised serious questions as to the accuracy of the view described above. Indeed, they suggest very strongly that the structure of the catalyst-Teflon layer is opposite to it. Scanning electron micrograph of electrodes and of dispersions of Pt-black, Teflon, and their mixtures in different

ratios have been made, and these reveal several significant details of the structure of the catalyst-Teflon layer as summarized below;

1) The Size, Shape, and Substructure of Teflon Particles

Scanning electron micrographs (SEM) of pure Teflon settled on a glass coverslide from a dilute dispersion revealed that Teflon particles are roughly prolate spheroidal in shape, but there is some evidence that these particles are aggregates of closely packed spheres as can be seen in Figure 2.2. The substructure of the Teflon particle is substantially more obvious in the SEM of catalyst-Teflon mixtures as seen in Figures 2.3 and 2.4, which are scanning electron micrographs of Pt-black-Teflon suspensions settled on filter paper and in Figure 2.5 which is a scanning electron micrograph of a fuel cell electrode. The increased visibility of the substructure may be due to the contrast provided by catalyst crystallites packing in the crevices between Teflon spheres.

If one assumes that the individual molecules are spherical, calculations by using mean molecular weight of 5 MM and density of 2.22 show that the size of a Teflon molecule ranges from 200 to 300 A in diameter.

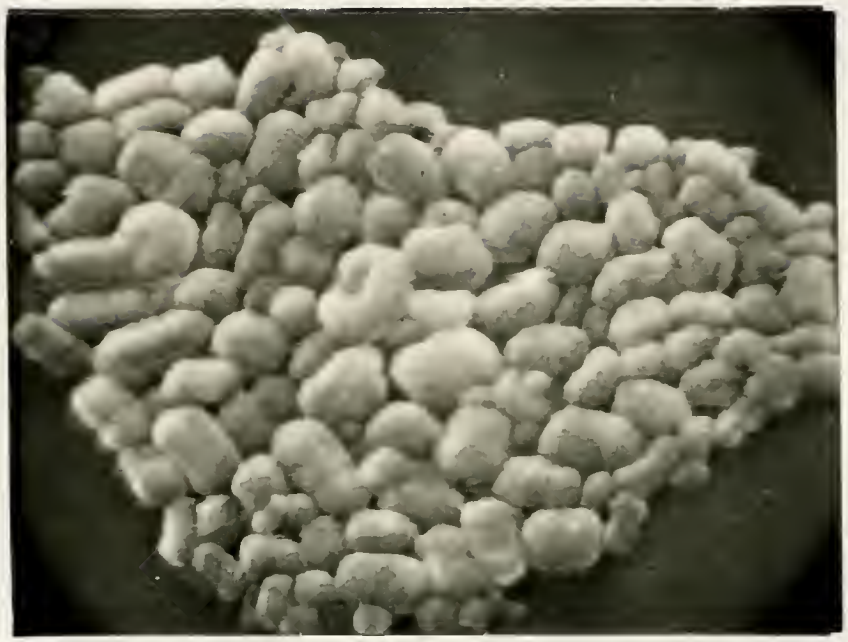

Figure 2.2: Scanning Electron Micrograph of Pure Teflon Particles. Magnification: 50,000.

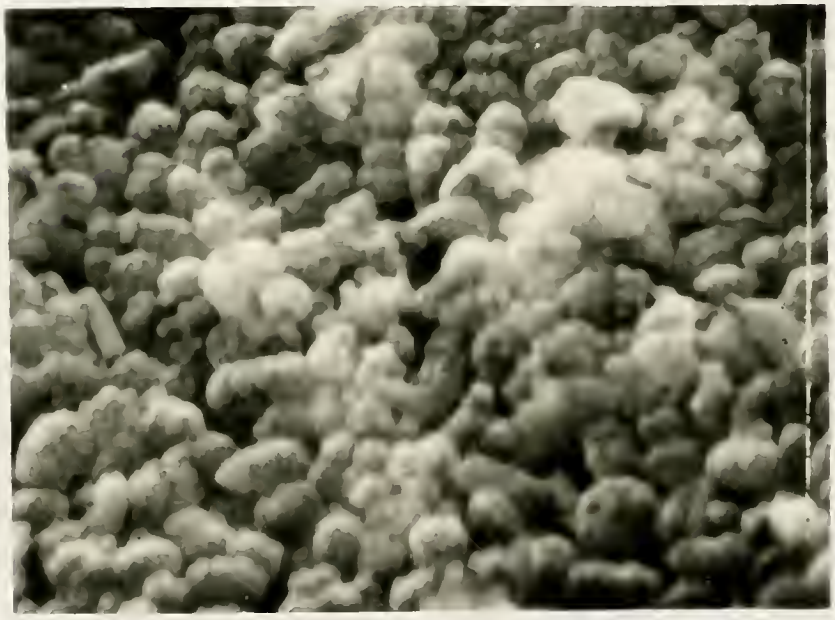

Figure 2.3: Scanning Electron Micrograph of Pt-black-Teflon Mixtures. Magnification: 36,000.

Figure 2.4: Scanning Electron Micrograph of Pt-black-Teflon Mixtures. Magnification: 72,000.

Figure 2.5: Scanning Electron Micrograph of a Fuel Cell Electrode. Magnification: 30,000.

2) Distribution of Pt-black in the Catalyst-Teflon Layer

It has been noted earlier that scanning electron microscopy has not resolved individual catalyst crystallites, but electron micrographs of catalyst-Teflon mixtures suggest very strongly that the catalyst particles coat the surface of the Teflon aggregates.

At large catalyst-Teflon ratios (Pt > 80 wt. %) multiple layers of catalyst particles appear to coat the surface of the Teflon aggregates and to fill the interstices between them. This phenomenon appears to be further substantiated by the fact that Teflon particles are negatively charged and Pt-black particles are positively charged. They would, therefore, be attracted to each other. This view of the catalyst-Teflon layer is illustrated in the diagrams below.

TEFLON AGGREGATE

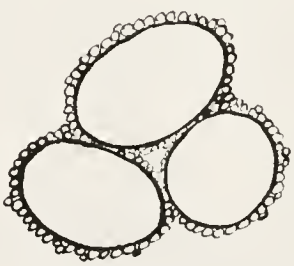

CATALYST-TEFLON MIXTURE

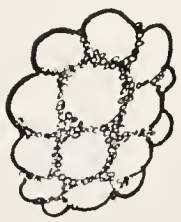

TENDENCY OF CATALYST TO FIRST COLLECT IN CREVICES BETWEEN TEFLON MOLECULES

3) Particle Packing and Pore Structure

The packing arrangement seems to be very close among Teflon molecules in an aggregate, and there were obviously macropores existing in a more or less random manner.

In order for porous gas diffusion electrodes to be effective there must be an appropriate amount of catalyst which, after being wetted by electrolyte, provides reaction sites for the heterogeneous electrochemical reactions. Moreover, the catalyst layer must also provide electron conduction paths, liquid phase mass transfer paths for reactants and products, and gaseous flow paths. When the proportion of catalyst in the catalyst-Teflon layer is too great, the catalyst will form a more or less continuous matrix so that Teflon particles will exist as isolated "islands," in which condition there would be no continuous gaseous channels within the catalyst Teflon layer. This would cause very limited utilization of the electrodes owing to the large gas diffusion resistance, i.e., almost all reaction would occur near the electrode-gas interface, resulting in a sharp decrease in electrode efficiency. On the other hand, when there exists too high a proportion of Teflon, the distribution of catalyst, as well as electrolyte paths, may be discontinuous, in which circumstance the

reactions would occur mostly on the electrolyte matrix side of the electrode, which is also another inefficient use of the electrodes.

Considering the previous two extreme cases, there ought to be a certain intermediate electrode composition in which there is enough catalyst to allow a continuous electrolyte phase and continuous paths for electron conduction, and enough Teflon so that there will be adequate continuous paths for the transfer of gaseous reactants. Industrially, electrodes with 80 wt. % Pt-black have been considered near optimal and are most widely used, but no entirely adequate modeling of these electrodes has yet been achieved. There exists a need to identify all transport processes occurring in operating electrodes and to devise a mathematical model of an electrode which will make it possible to correlate known electrode behavior with the predictions of the model, and to design improved electrodes.

CHAPTER III

ELECTRODE REACTIONS, IONIC HYDRATION, AND WATER TRANSPORT

3.1 Introduction

Alkaline fuel cells, as pointed out by Kordesch [6], are technologically the most advanced fuel cell type today. Despite their high power output and increasingly lower cost, many problems remain to be solved before they can have extensive commercial applications. The concentration gradients of electrolyte in the matrix of an operating fuel cell have been measured by Miller and Fornasar [7], and by Lundquist and Vogel [8]. However, the transport of free water within the electrolyte matrix has not been discussed in the literature. In this chapter we will look into the problem of water transport in the electrolyte matrix in relation to electrode reactions and ionic hydration to develop ways of estimating the concentration gradients of free water and the electrolyte in the matrix.

The overall reaction product in the alkaline hydrogen-oxygen fuel cell is water. Water generated by this reaction must be removed from the cell to avoid dilution of the electrolyte, but water transport within the fuel cell is also very important in another sense: it is both a reactant at

the cathode and a solvator of the hydroxyl ions formed there. The reactions at the electrodes can be written as follows:

Anode reaction: $2\ H_2 + 4[OH^- \cdot s\ H_2O] = 4(1+s)\ H_2O + 4e$

Cathode reaction: $O_2 + 2(1+2s)\ H_2O + 4e = 4[OH^- \cdot s\ H_2O]$

Overall reaction: $2H_2 + O_2 = 2H_2O$

where s is the primary hydration number of the hydroxyl ion.

It can be seen that water must be transferred to the cathode both to maintain the cathode reaction and to solvate the hydroxyl ions produced there. Water transport from the anode to the cathode involves transport of solvent water whereas water transport from the cathode to the anode involves transport of hydrated hydroxyl ions.

All of the ions in the electrolyte are hydrated but our principal concern is with the hydroxyl ions as these carry most of the intracell current and they participate in the electrode reactions, whereas potassium ions do not. As pointed out by Bockris [9], water may be regarded as being bound to ions in two ways: (i) strongly bound and (ii) weakly bound. Strongly bound water - called the primary hydration sheath - is held so strongly to ion that it moves with the ion. Weakly bound water - called the secondary hydration sheath - is attached so loosely to the ions that it behaves like a diffuse cloud around the ion and is in continuous interchange with water in the surrounding

medium. Only the primary hydration sheath will be considered here. The number of water molecules in the primary hydration sheath of an ion is called the primary hydration number of the ion.

3.2 Mass Transfer in the Electrolyte Matrix

The electrolyte matrix usually consists of a thin sheet of specially processed asbestos with the voids between the asbestos fibers being filled with electrolyte, which, in this case, is concentrated potassium hydroxide. All transport takes place in the electrolyte solution which has three constituents: water, potassium, and hydroxyl ions. However, these ions do not exist as bare ions: rather, they exist as solvated ions and the water in the primary hydration sheath around the ion is fairly tightly bound so that it moves with the ion.

As the hydrated hydroxyl ion moves from a region of high KOH concentration to one of low KOH concentration, the hydration number increases and a relationship of the following form can be written:

$$OH^- \cdot s_1 H_2O + (s_2 - s_1)\ H_2O = OH^- \cdot s_2 H_2O$$

Since the KOH concentration in a fuel cell is usually large and since according to Bockris and Saluja [10] the hydration number appears to change slowly with KOH concentration in this concentration range, it can be assumed that $s_2 - s_1$ is

small so that an average value s can be used over the entire electrolyte matrix.

In a multicomponent system the momentum flux depends only upon the velocity gradients and the energy flux depends upon the temperature gradient. In the electrolyte matrix considered, although there may be some local variations in temperature, the temperature differences across the matrix are small compared to the absolute temperature. Therefore constant temperature will be assumed in the electrolyte matrix. Also, because the electrolyte is contained in the small void spaces of the electrolyte matrix, convection will be assumed to be absent, i.e., the bulk velocity of the fluid in the matrix is zero. Hence, it is not necessary to consider the equations of motion and energy.

The mass or molar flux of a species depends both on mechanical driving forces (ordinary, pressure, and forced diffusion) and on thermal diffusion effects. The multicomponent diffusion equation is [11]:

$$C_i\left[\nabla\mu_i + \bar{s}_i\nabla T - \frac{M_i}{\rho}\nabla P\right] = RT\sum_j \frac{C_iC_j}{C_T\mathcal{D}_{ij}}\left[(v_j-v_i) + \left(\frac{D_j^T}{\rho_j} - \frac{D_i^T}{\rho_i}\right)\nabla \ell nT\right] \qquad (3.1\text{-}1)$$

where μ_i = electrochemical potential of species i, Joule/mole;

$\bar{s}_i$ = partial entropy of species i, Joule/mole-deg;

$\mathcal{D}_{ij}$ = diffusion coefficient of i in j, cm^2/sec;

D_i^T = thermal diffusion coefficient of i, gm/cm-sec;

C_T = total solution concentration, mole/l;

v_i = average velocity of species i, cm/sec.

It was already assumed that the temperature in the electrolyte matrix is constant and the gradient of pressure is usually very small. Thus, the thermal diffusion and the pressure diffusion terms are usually of only secondary importance and may be neglected. Equation (3.3-1) then takes the form

$$C_i \nabla \mu_i = RT \sum_j \frac{C_i C_j}{C_T \mathcal{D}_{ij}} (v_j - v_i) \qquad (3.3\text{-}2)$$

The $\mathcal{D}_{ij}$ are the diffusion coefficients describing the interactions between species i and j. For potassium hydroxide solutions we have two independent equations

$$C_+ \nabla \mu_+ = RT \left[\frac{C_+ C_o}{C_T \mathcal{D}_{o+}} (v_o - v_+) + \frac{C_- C_+}{C_T \mathcal{D}_{-+}} (v_- - v_+) \right] \qquad (3.3\text{-}3)$$

$$C_- \nabla \mu_- = RT \left[\frac{C_- C_o}{C_T \mathcal{D}_{o-}} (v_o - v_-) + \frac{C_- C_+}{C_T \mathcal{D}_{-+}} (v_+ - v_-) \right] \qquad (3.3\text{-}4)$$

where C_o = concentration of total free water, moles/l;

C_+ = concentration of potassium ion, moles/l;

C_- = concentration of hydroxyl ion, moles/l;

C_T = total solution concentration, moles/l;

μ_+ = electrochemical potential of the potassium ion, Joule/mole;

μ_- = electrochemical potential of the hydroxyl ion, Joule/mole.

The flux equations for the potassium ion and the hydroxyl ion may be obtained by rearranging Equations (3.3-3) and

(3.3-4). For steady-state conditions, these flux equations can be written as follows (see Appendix 1 for details):

$$\underline{N}_+ = C_+\underline{v}_+ = -\frac{\nu_+ \mathcal{D} C_T C}{\nu RTC_o}\nabla\mu_e + \frac{it_+}{z_+F} + C_+\underline{v}_o \qquad (3.3\text{-}5)$$

$$\underline{N}_- = C_-\underline{v}_- = -\frac{\nu_- \mathcal{D} C_T C}{\nu RTC_o}\nabla\mu_e + \frac{it_-}{z_-F} + C_-\underline{v}_o \qquad (3.3\text{-}6)$$

where $\mathcal{D}$ is the diffusion coefficient of the electrolyte and is given by

$$\mathcal{D} = \frac{\mathcal{D}_{o+}\mathcal{D}_{o-}(z_+ - z_-)}{z_+\mathcal{D}_{o+} - z_-\mathcal{D}_{o-}} \qquad (3.3\text{-}7)$$

and v_o is the diffusion velocity of water. The transference numbers (with respect to the solvent velocity) are defined as follows:

$$t_+ = 1 - t_- = \frac{z_+\mathcal{D}_{o+}}{z_+\mathcal{D}_{o+} - z_-\mathcal{D}_{o-}} \qquad (3.3\text{-}8)$$

The measured diffusion coefficient, D, is related to $\mathcal{D}$ by

$$D = \frac{\mathcal{D} C_T}{C_o}\left[1 + \frac{d\ \ell n\ \gamma_\pm}{d\ \ell n\ m}\right] \qquad (3.3\text{-}9)$$

where $\gamma_\pm$ is the mean molal activity coefficient and m is the molality.

It can be shown that the relation between the gradient of chemical potential and the gradient of concentration is given by (see Appendix 2)

$$\frac{\mathcal{D}C_T C}{\nu RTC_o} \nabla\mu_e = D\left[1 - \frac{d\ \ell n\ C_o}{d\ \ell n\ C}\right] \nabla C \qquad (3.3\text{-}10)$$

Substitution of Equation (3.3-10) into Equations (3.3-5) and (3.3-6) gives

$$\underline{N}_+ = -\nu_+ D\left[1 - \frac{d\ \ell n\ C_o}{d\ \ell n\ C}\right] \nabla C + \frac{it_+}{z_+ F} + C_+ \underline{v}_o \qquad (3.3\text{-}11)$$

and

$$\underline{N}_- = -\nu_- D\left[1 - \frac{d\ \ell n\ C_o}{d\ \ell n\ C}\right] \nabla C + \frac{it_-}{z_- F} + C_- \underline{v}_o \qquad (3.3\text{-}12)$$

For water, the total flux consists of the flux due to free water, that due to water of hydration, and that due to convection. Since potassium ions do not enter into the electrode reactions, the net flux of potassium ions is zero and the flux of hydration water with potassium ions is zero. Thus, we have

$$\underline{N}_{H_2O} = -D\nabla C_{fw} + s\underline{N}_- + C_o \underline{v}_o \qquad (3.3\text{-}13)$$

where C_{fw} is concentration of free water.

It was already assumed that all transport is essentially one-dimensional, so the flux equations become

$$\underline{N}_- = -\nu_- D\left[1 - \frac{d\ \ell n\ C_o}{d\ \ell n\ C}\right] \nabla C + \frac{it_-}{z_- F} + C_- \underline{v}_o \qquad (3.3\text{-}14)$$

$$\underline{N}_{H_2O} = -D \frac{dC_{fw}}{dx} + s\underline{N}- \qquad (3.3\text{-}15)$$

In order to solve these equations, it is necessary to know the transference number and the hydration number of ions.

3.3 Transference Numbers in KOH Solutions

The transference number of an ion is the fraction of the total current carried by that ion. Several methods for measuring transference numbers are known and several empirical equations for transference number as a function of concentration have been developed. However, most of the aforementioned studies have been done intensively on dilute solutions and studies in concentrated electrolytic solutions have been less frequent. Among the empirical equations is the Onsager equation, according to which the equivalent conductance of an ion, λ_i, is given by

$$\lambda_i = \lambda_i^o - \left(\frac{1}{2} A + B\lambda_i^o\right)\sqrt{C} \qquad (3.3\text{-}16)$$

where λ_i^o = ionic conductance of species i at infinite dilution, cm^2/ohm;

A,B = constants.

Thus, the transference number of the potassium ion is given by

$$t_+ = \frac{\lambda_+}{\lambda_+ + \lambda_-} = \frac{\lambda_+^o - (\frac{1}{2} A + B\lambda_+^o)\sqrt{C}}{\Lambda^o - (A + B\Lambda^o)\sqrt{C}} \qquad (3.3\text{-}17)$$

where $\Lambda^o = \lambda_+^o + \lambda_-^o$.

While the Onsager theory predicts the concentration dependence of the transference number, it is applicable only at low concentrations.

Recently, Merenkov [12] measured the transference number of potassium in KOH solutions of high concentrations. It was found that the transference number of potassium ion was independent of temperature from 18 to 65 °C but that it decreased with increase in KOH concentration. The transference number of potassium ion was correlated by the empirical equation

$$t_+ = 0.260 - 0.047(\sqrt{C} + 1) \qquad (3.3\text{-}18)$$

On the other hand, Knobel [13] determined the transference number of the potassium ion in KOH solutions by the EMF method; he found that the transference number of potassium was 0.2633 and that it was independent of concentration over the concentration range from 0.03 to 3.0 N. The predictions of the Onsager theory and the experimental results of Knobel and Merenkov are summarized in Table 3.1.

In fuel cell operations concentrated solutions of KOH are used. Therefore, the Merenkov's data, which are the only ones available for high concentrations, will be used in the later calculations.

3.4 The Primary Hydration Numbers in Concentrated KOH Solutions

The hydration number of an ion is the number of water molecules attached to the ion, and the absolute value of the

Table 3.1

Summary of Transference Number Data for KOH Solutions.

Concentration of KOH Solutions (N)	Transference Number of K^+ from		
	Onsager Eq.	Knobel	Merenkov
0.03	0.261	0.2633	0.205
0.1	0.251	0.2633	0.198
0.3	0.232	0.2633	0.187
1.0	0.176	0.2633	0.166
3.0	-	0.2633	0.132
5.0	-	-	0.108
7.0	-	-	0.088
9.0	-	-	0.072
10.0	-	-	0.064

hydration number has an important bearing on the amount of "free" water present in the electrolytic solutions. For example, in 30 wt. % KOH solution, if the hydration number of both the potassium and hydroxyl ions is equal to one, then the concentration of "free" water is 36.4 moles/l, while if the hydration number of the ions is equal to four, there will not be any "free" water available. The concentration of "free" water for different values of the hydration number at various KOH concentrations is tabulated in Table 3.2 (assuming that the hydration number of the potassium ion is equal to that of the hydroxyl ion) and shown in Figure 3.1 as a function of KOH concentration.

Table 3.2

Concentration of "Free" Water
as a Function of Hydration Number.

Concentration of KOH Solution		Concentration of Free Water, C_{fw}, moles/l					
wt. %	Moles/l	s = 0	1	2	3	4	5
10	1.91	53.58	49.76	45.93	42.11	38.29	34.46
20	4.16	51.81	43.49	35.16	26.84	18.52	10.20
30	6.80	49.27	35.67	22.08	8.48	-	-
40	9.86	45.87	26.14	6.41	-	-	-
50	13.44	41.52	14.65	-	-	-	-

The concept of ionic hydration has been investigated by many workers and several experimental methods have been used for determining the hydration number of ions. However, the different experimental methods give contradictory results because of a lack of a really precise definition of the hydration number. Recently, Bockris [10] used the compressibility method to determine the sum of the hydration numbers of ions in solutions of halides. By combining compressibility measurements of the ionic vibration potential, individual hydration numbers for certain cations and anions were estimated. According to these results, the hydration number of potassium ion in dilute solutions is 3.5 while that for hydroxyl ion can be estimated to be equal to 4.3. If these hydration numbers remain constant in concentrated solutions, as pointed out earlier, there would not be any "free" water available in

Figure 3.1: Concentration of "Free" Water for Different Values of Hydration Number.

30 wt. % KOH solution. It is obvious, therefore, that the hydration number must vary with the concentration of the solution, but there is little experimental information concerning the concentration dependence of the hydration numbers of the potassium and hydroxyl ions at high concentrations.

From some of the limited information available in Bockris' paper [10], the hydration number of the potassium and hydroxyl ions may be estimated by extrapolating the data available. This procedure results, for 30 wt. % KOH solution, in an estimated hydration number of potassium ion of 2.0 and 2.0 for the hydroxyl ion. These values are, however, very tentative owing to the extrapolation required. Since they are the best estimates available, they are used in the next section to estimate concentration gradient in the electrolyte matrix for different current densities.

3.5 Concentration Gradients in the Electrolyte Matrix

Having estimated the hydration numbers and the transference numbers of the ions, the flux equations for the potassium ion, the hydroxyl ion, and water can be solved. The concentration gradients of the "free" water and that of the electrolyte in the electrolyte matrix can be estimated as follows:

3.5.1 Concentration Gradients of "Free" Water

For the "free" water concentration gradients in the x-direction, we have from Equation (3.3-15)

$$N_{H_2O,x} = -D \frac{dC_{fw}}{dx} + sN_{-,x} \qquad (3.3\text{-}15)$$

From the electrode reactions at both anode and cathode it can be seen that the flux of "free" water from the anode to the cathode is one-half of the hydroxyl ion flux in opposite direction. Therefore, the following can be written.

$$N_{H_2O,x} = -D \frac{dC_{fw}}{dx} + sN_{-,x} = -N_{-,x}/2 \qquad (3.5\text{-}1)$$

Since, according to the Faraday's law, $N_{-,x} = \frac{i}{z_- F}$, the "free" water concentration gradient can be expressed in terms of the hydration number of ions, the diffusivity, and the current density, that is

$$\frac{dC_{fw}}{dx} = \left(s + \frac{1}{2}\right) \frac{i}{z_- DF} \qquad (3.5\text{-}2)$$

Values of the diffusion coefficient of the electrolyte at various concentrations, taken from Bhatia's results [14], are converted into the molar average frame (see Appendix 3). With the available data on diffusivity and the various values of the hydration number, the concentration gradients of the "free" water at different KOH concentrations can be calculated as a function of current density. The results of "free" water concentration gradients are summarized in Table 3.3.

3.5.2 Concentration Gradients of KOH Solution

For the concentration gradient of the KOH solution, we have from Equation (3.3-14)

Table 3.3

"Free" Water Concentration Gradients.

Hydration No. of Hydroxyl ion, s	KOH Concentration, C, moles/l				
	1.91	4.16	6.80	9.86	13.44
0	0.085i	0.078i	0.075i	0.074i	0.071i
1	0.236i	0.199i	0.171i	0.143i	0.110i
2	0.365i	0.274i	0.221i	0.108i	-
3	0.470i	0.303i	0.202i	-	-
4	0.552i	0.285i	-	-	-
5	0.610i	0.220i	-	-	-

$$N_{-,x} = -\nu D\left(1 - \frac{d\ \ell n\ C_{fw}}{d\ \ell n\ C}\right)\frac{dC}{dx} + \frac{it_-}{z_-F} + C_-v_{o,x} \qquad (3.5\text{-}3)$$

Since $N_{-,x} = \frac{i}{z_-F}$, $1 - t_- = t_+$, and $N_{H_2O,x} = -\frac{N_{-,x}}{2} = C_{fw}v_{o,x}$, Equation (3.5-3) yields

$$\frac{dC}{dx} = -\frac{i}{z_-F}\left(t_+ + \frac{C_-}{2C_{fw}}\right)/\nu_-D\left(1 - \frac{d\ \ell n\ C_{fw}}{d\ \ell n\ C}\right) \qquad (3.5\text{-}4)$$

The term $\left(1 - \frac{d\ \ell n\ C_{fw}}{d\ \ell n\ C}\right)$ can be shown to be equal to $\frac{1}{C_{fw}\ \bar{V}_o}$, where $\bar{V}_o$ is the partial molal volume of the solvent water and is given by

$$\bar{V}_o = \frac{M_o}{\rho - C\frac{d\rho}{dC}} \qquad (3.5\text{-}5)$$

where M_o = molecular weight of water.

Therefore, Equation (3.5-4) becomes

$$\frac{dC}{dx} = - \frac{C_{fw} M_o \left(t_+ + \frac{C_o}{2C_{fw}} \right)}{\nu_- z_- DF \left(\rho - C \frac{d\rho}{dC} \right)} i \qquad (3.5\text{-}6)$$

As for the density-concentration relation of KOH solution, an equation that relates the density with the concentration has been developed from the density-concentration data[15] by using the Lagrange interpolation formula.

$$\rho(C) = 1.00086 + C(0.04930 - C(0.0143 - C(0.000059 - 0.0000014C))) \qquad (3.5\text{-}7)$$

Differentiation of Equation (3.5-7) gives

$$\frac{d\rho}{dC} = 0.04930 - C(0.00286 - C(0.000177 - 0.0000056C)) \qquad (3.5\text{-}8)$$

The concentration gradients of KOH solution calculated from Equation (3.5-6) are summarized in Table 3.4.

3.6 Discussion

From Table 3.4 it can be seen that, for the estimated values of the transference and hydration numbers, a current density of one ampere per cm^2, and a mean KOH concentration of 30 wt. % (= 6.80 N), the KOH concentration gradient in the electrolyte matrix is 0.009 gmole/l-cm. Since the electrolyte matrix is normally less than one millimeter in thickness, it seems clear that the KOH concentration dif-

Table 3.4

KOH Concentration Gradients in Electrolyte Matrix.

Hydration No. of Hydroxyl Ion, s	KOH Concentration, C, moles/l			
	c = 1.91	4.16	6.80	9.86
1	0.0243i	0.0172i	0.0133i	0.0109i
2	0.0210i	0.0123i	0.0090i	0.0040i
3	0.0179i	0.0082i	0.0048i	-
4	0.0151i	0.0049i	-	-
5	0.0125i	0.0024i	-	-

ference between the anode and the cathode even at the high current density of one ampere per cm^2 appears to be almost negligible.

CHAPTER IV

MATHEMATICAL MODEL OF TEFLON-CATALYST LAYER AND CALCULATION OF CURRENT DENSITY DISTRIBUTION

4.1 Introduction

Investigation of the electrode structure by scanning electron microscopy (SEM) and energy dispersive X-ray analysis (EDXA) has yielded much information on how the platinum black catalyst and the Teflon particles are mixed to form the catalyst-Teflon layer of the electrode. On the basis of this information we can understand how the electrode is wetted, how gaseous reactants can be transported, and what the means of ionic, electronic, and water transport are. Mathematical modeling of these catalyst-Teflon layers has been done to relate these findings to predicted performance of the electrodes.

A scanning electron micrograph of the surface of a layer of Pt:Teflon in the weight ratio 80:20 is shown in Figure 4.1 (Magnification = 72,000). From studies of this and similar SEM the following conclusions can be drawn:

1) The Teflon aggregates are prolate spheroids of sizes 2000 to 3000 A in the major axis and 1000 to 1500 A in the minor axis. However, the substructure of these spheroids shows that they

consist of aggregates of spherical Teflon molecules with diameters of 200 to 300 A.

Figure 4.1: Scanning Electron Micrograph of the Surface of the 80:20 Pt-black-Teflon Layer. Magnification: 72,000 .

2) Owing to thin extremely small size the catalyst crytallites cannot be resolved in the SEM, but it is clear that they have an equivalent diameter of less than 100 A. From measurement of its surface area by the BET gas adsorption method and the estimation of its packing condition as shown in Chapter II, it seems very likely that the diameter of a single catalyst crystallite is in the range of 30 to 40 A.

3) The Teflon aggregates are coated with thin layers of catalyst crystallites and the distribution seems

to be relatively uniform. As the ratio of platinum black to Teflon increases, the chances of observing bare Teflon decrease, and the great majority of Teflon aggregates are coated by platinum black in the electrode of 80:20 platinum black-Teflon mixture

From these observations it appears that the following processes occur during the formation of an electrode:

1) When a well-dispersed suspension of platinum black is mixed with Teflon 30 dispersion (which is negatively charged hydrophobic colloid), the Teflon aggregates are coated with platinum black.
2) During the filtration of this mixture the catalyst-coated aggregates settle on the filter medium and form a layer of platinum black-coated Teflon particles.
3) When the filter cake is pressed, these particles are compacted together very tightly.
4) During the sintering process, the Teflon aggregates expand, soften, and contact one another to form a bonded layer with more or less continuous structure.

On the basis of these observations and conjectures the electrode can be pictured as consisting of gas channels of varying cross section through the intra-aggregate voids of the Teflon aggregates which are themselves coated with a catalyst layer on their external surface. This catalyst

layer is wetted and penetrated by the electrolyte. Thus, gas penetrates the catalyst-Teflon layer by means of the intra-aggregate voids and electrolyte penetrates the extra-aggregate voids where the catalyst crystallites lie. Gas, electrolyte, and catalyst meet at the surface of the Teflon aggregates as shown schematically in cross section in Figure 4.2.

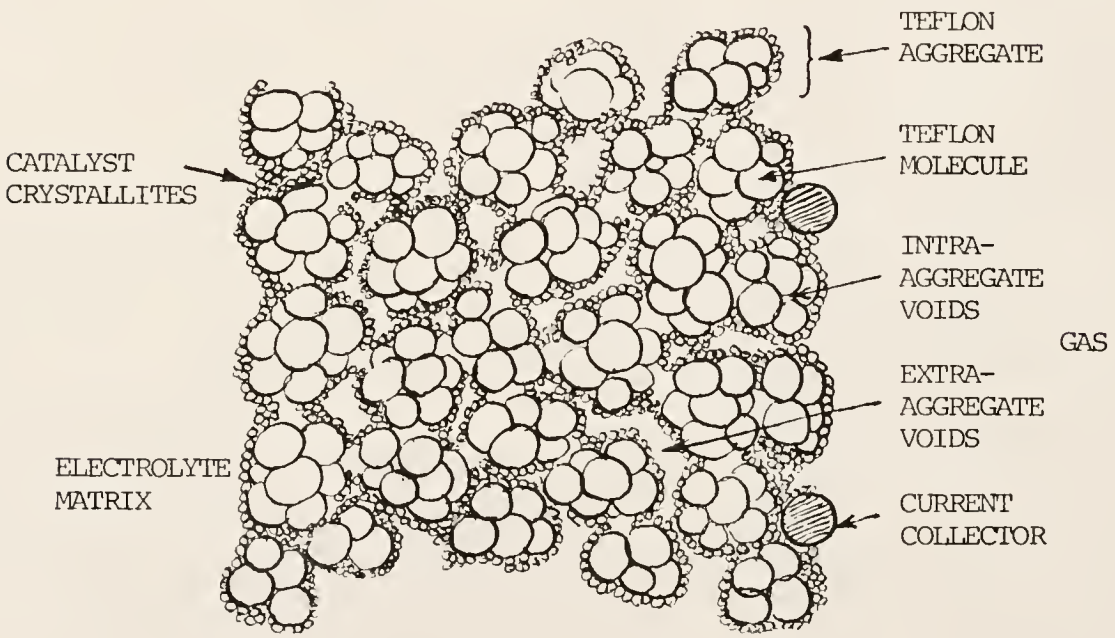

Figure 4.2: Schematic Diagram of Platinum Black Catalyst and Teflon Particles in Electrodes.

A cylindrical multicompartment model as shown in Figure 4.3 is a much simplified but fairly reasonable approximation of the structure of the catalyst-Teflon layer. A compartment in the model represents a Teflon aggregate which consists of several Teflon molecules and interconnected intra-aggregate voids. Windows represent narrow gas-phase connec-

tions between Teflon aggregates which may limit the transport of gaseous reactants.

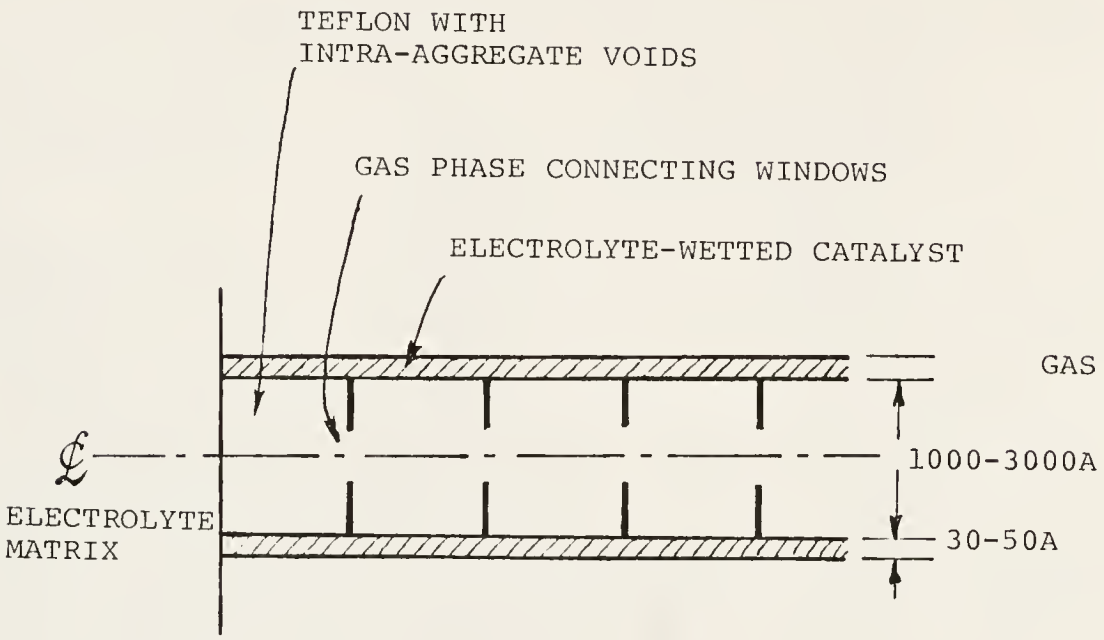

Figure 4.3: Schematic Model of the Structure of the Catalyst-Teflon Layer.

Although the model described above represents the structure of electrode layer very well, there arises a problem in mathematical modeling due to the existence of the windows which limit the transport of gaseous reactants. For the sake of simplicity in mathematical modeling and due to the limitation in time, the model shown in Figure 4.4, which is the same as the multicompartment model except having no windows, is adopted for this work.

For an electrode modeling only the oxygen electrode was considered because the limiting current density of a hydrogen-oxygen fuel cell is usually determined by the oxygen electrode

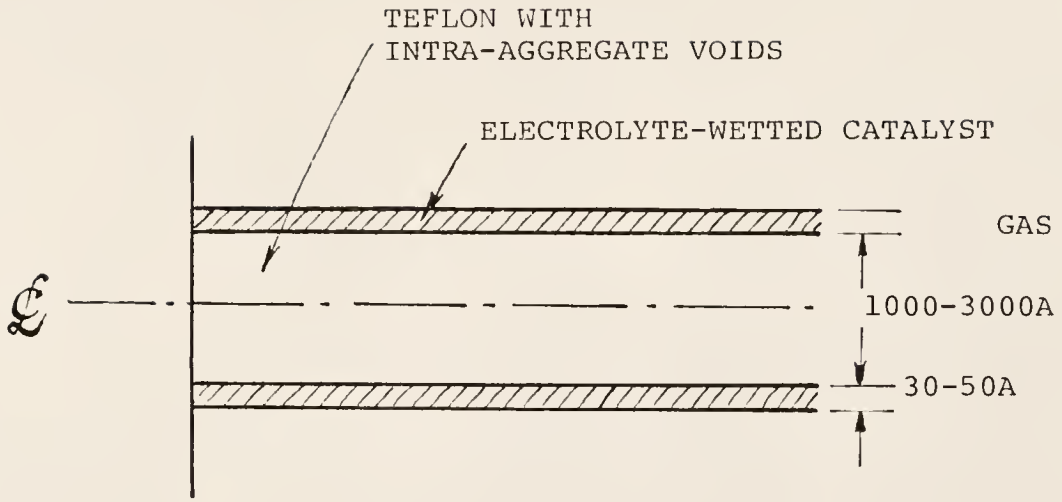

Figure 4.4: Schematic Model of the Structure of the Catalyst-Teflon Layer with No Windows.

owing to the slowness of the reduction of oxygen on the catalyst surface. The following assumptions were made in the development of the mathematical model to simplify the computations:

1) Steady state, i.e., constant current density.
2) Isothermal.
3) Diffusion coefficients and other physical properties are independent of electrolyte concentration.
4) Potential and current are assumed to vary in the x-direction only.

5) The concentration of KOH is assumed to vary in the x-direction only.

6) The diffusion of oxygen through gaseous space is not restricted.

7) Both cations and anions have same primary hydration number. In this work it is taken to be 2.

4.2 Electrode Reaction and Reaction Rate

The electrochemical reaction in the oxygen electrode may be written as

$$O_2 + 10\ H_2O + 4\ e^- \rightarrow 4[OH^- \cdot 2H_2O]$$

For convenience we denote $OH^- \cdot 2H_2O$, $K^+ \cdot 2H_2O$, O_2, and H_2O as species 1, 2, 3, and 4, respectively, in the equations which follow.

Although several workers [16,17] have studied the mechanism of the reduction of oxygen in alkaline solutions on platinum catalysts, it is still inadequately understood. However, the work of Gnanamuthu and Petrocelli [18] suggested that a suitable rate equation is

$$\frac{di_s}{dx} = \alpha i_o \left[\left(\frac{C_3(x)}{C_3^o} \right) \left(\frac{C_4(x)}{C_4^o} \right) \exp(-F(\phi_s - \phi_\ell)/RT) - \left(\frac{C_1(x)}{C_1^o} \right) \exp(F(\phi_s - \phi_\ell)/RT) \right] \qquad (4.2\text{-}1)$$

where i_s = current density in the catalyst phase, amp/cm^2;

α = surface area per unit volume of electrode, cm^2/cm^3;

i_o = exchange current density, amp/cm^2;

C_i = concentration of species i, gmole/l;

C_i^o = concentration of species i at x = 0, gmole/l;

ϕ_s = potential in the catalyst phase, volt;

ϕ_ℓ = potential in the electrolyte phase, volt.

Equation 4.2-1 must be solved with the following boundary conditions:

$$\text{At } x = 0, \qquad i_s = 0$$

$$\text{At } x = L, \qquad i_s = i_{app}$$

where i_{app} = apparent current density being drawn from the electrode, amp/cm^2.

4.3 Ionic Fluxes in the Electrolyte Phase

At steady state the mass fluxes in the x-direction for a binary electrolyte system can be written as [19]

$$N_{1,x} = - \frac{\mathcal{D}^* \nu_1 C}{\nu RT} \frac{d\mu_e}{dx} + \frac{i_\ell t_1^*}{z_1 F} + C_1 v_{1,x}^* \qquad (4.3\text{-}1)$$

$$N_{2,x} = 0 = - \frac{\mathcal{D}^* \nu_2 C}{\nu RT} \frac{d\mu_e}{dx} + \frac{i_\ell t_2^*}{z_2 F} + C_2 v_{2,x}^* \qquad (4.3\text{-}2)$$

where $N_{1,x}$ and $N_{2,x}$ are fluxes of hydroxyl and potassium ions.

Since $C_T = C_1 + C_2 + C_4 = 2C + C_4$,

$$C_T v_x^* = C_1 v_{1,x} + C_2 v_{2,x} + C_4 v_{4,x} = C_1 v_{1,x} + C_4 v_{4,x} ,$$

$$C_1 v_{1,x} = N_{1,x} = -i_\ell / F, \text{ and}$$

$$C_4 v_{4,x} = N_{4,x} = -N_{1,x}/2 ,$$

Equation (4.3-2) can be rearranged to give

$$\frac{\mathcal{D}^* \nu_2 C}{\nu RT} \frac{d\mu_e}{dx} = \frac{i_\ell}{F} \left(\frac{t_2^*}{z_2} - \frac{C}{C_T} \right) \tag{4.3-3}$$

Since $\mu_e = \nu RT \ell na$, $z_2 = 1$, and $D^* = \frac{D^V}{(C+C_4)\bar{V}_4} = \mathcal{D}^* \frac{d\ell na}{d\ell nC}$ (see Appendix 3), Equation (4.3-3) becomes

$$\frac{\nu_2 C D^V}{(C+C_4)\bar{V}_4} \frac{d\ell nC}{dx} = \left(t_2^* - \frac{C}{C_T} \right) \frac{i_\ell}{F} \tag{4.3-4}$$

Substitution of $t_2^* = \frac{C+C_4 t_2}{C_T}$ into Equation (4.3-4) gives

$$\frac{dC}{dx} = \frac{i_\ell t_2 C_4 \bar{V}_4}{F D^V C_T} (C + C_4) \tag{4.3-5}$$

which will be solved by using one of the boundary conditions, namely, at $x = 0$, $C = C_o$.

4.4 Potential Gradients in the Electrode Layer

The potential drop in the catalyst phase is governed by Ohm's law

$$i_s = -\sigma \frac{d\phi_s}{dx} \tag{4.4-1}$$

where σ is the conductivity of catalyst.

The current carried by the ions is related to the potential ϕ_ℓ by the following equation [20]

$$i_\ell = \kappa \frac{d\phi_\ell}{dx} - \frac{\kappa}{F}\left(\frac{s_2}{n\nu_2} + \frac{t_2}{z_2\nu_2} - \frac{s_4 C}{nC_4}\right)\frac{d\mu_e}{dx} \qquad (4.4\text{-}2)$$

where κ is the conductivity of the electrolyte and s_i is the stoichiometric coefficient of species i in the equation

$$s_1 M_1^{z_1} + s_2 M_2^{z_2} + s_4 M_4 \rightarrow ne^-$$

Substituting $\mu_e = \nu RT\ell na$ into Equation (4.4-2) for the electrode reaction equation gives

$$\frac{d\phi_\ell}{dx} = -\frac{i_{app} - i_s}{\kappa} - \frac{\nu RT}{nF}\left(t_2 + \frac{2.5C}{C_4}\right)\frac{d\ell na}{d\ell nC}\frac{dC}{dx} \qquad (4.4\text{-}3)$$

Equations (4.4-1) and (4.4-3) can be solved with two B.C.'s, i.e., at $x = 0$, $\phi_s = 0$, and at $x = L$, $i_s = i_{app}$.

4.5 Oxygen Transport in the Electrolyte Phase

The concentration of oxygen in the electrolyte phase will vary both in the r- and x-directions. In work by Tham [21], ϕ_ℓ, ϕ_s, C_1, C_2, and C_4 were assumed to vary in the x-direction only, and these led to predicted current densities which agreed reasonably well with experimental values, i.e., radial concentration gradients appeared to be relatively small. To evaluate the variation of $C_3(r,x)$ for a given x, an average value of $\bar{C}_3(x)$ was evaluated at that x.

The flux equation for oxygen is

$$D_3 \frac{d^2C_3}{dr^2} + \frac{D_3}{r}\frac{dC_3}{dr} - \frac{1}{nF}\frac{di_s}{dx} = 0 \qquad (4.5\text{-}1)$$

where $\frac{di_s}{dx}$ is given by Equation (4.2-1).

After several mathematical operations (see Appendix 4), the following equation was obtained for $\bar{C}_3(x)$.

$$\frac{\bar{C}_3(x)}{C_3^o} = \frac{C_1(x)C_4^o}{C_1^o C_4(x)} \exp\left[\frac{2F(\phi_s-\phi_\ell)}{RT}\right] + \frac{2r_o}{q(DEN)}$$

$$x \left[1 - \frac{C_1(x)C_4^o}{C_1^o C_4(x)} \exp\left[\frac{2F(\phi_s-\phi_\ell)}{RT}\right]\right]$$

$$x \left(I_1(q(r_o+\delta))K_1(qr_o) - K_1(q(r_o+\delta))I_1(qr_o)\right) \frac{1}{(2r_o\delta+\delta^2)} \qquad (4.5\text{-}2)$$

where $q^2 = \frac{\alpha i_o}{nFC_3^o D_3} \frac{C_4(x)}{C_4^o} \exp\left[-\frac{F(\phi_s-\phi_\ell)}{RT}\right]$;

I_o, K_o = Bessel functions of zero order;

I_1, K_1 = Bessel functions of first order;

$DEN = K_1(q(r_o+\delta))I_o(qr_o) + K_o(qr_o)I_1(q(r_o+\delta))$.

Substitution of the average value of $\bar{C}_3(x)$ for $C_3(x)$ into Equation (4.2-1) gives

$$\frac{di_s}{dx} = \alpha i_o \left(\frac{\bar{C}_3(x)}{C_3^o}\frac{C_4(x)}{C_4^o} \exp\left[-\frac{F(\phi_s-\phi_\ell)}{RT}\right] - \frac{C_1(x)}{C_1^o} \exp\left[\frac{F(\phi_s-\phi_\ell)}{RT}\right]\right) \qquad (4.5\text{-}3)$$

To solve for $C(x)$, $C_3(x)$, $i_s(x)$, $\phi_s(x)$, and $\phi_\ell(x)$, Equations (4.3-5), (4.4-1), (4.4-3), (4.5-2), and (4.5-3) can be combined with the accompanying boundary conditions.

4.6 Computation of the Current Generation

Equations (4.3-5), (4.4-1), (4.4-3), (4.5-2) and (4.5-3) were integrated numerically using the quadratic Runge-Kutta method; the computer program for the computation of the current density distribution is given in Appendix 5. Numerical values of the properties of the electrolyte such as electrolytic conductivity, partial molal volume, and the activity of the electrolyte, and other necessary terms were expressed in the form of polynomial equations as functions of the KOH concentration. The specific conductance of KOH was taken from the data by Klochko and Godneva [22] and was expressed in a polynomial form by using the Lagrange interpolation formula as follows:

$$\kappa = -0.59876 + C(0.608757 - C(0.0684246 - 0.00229369C)) \qquad (4.6\text{-}1)$$

In the calculation of current generation the specific surface area of Pt-black catalyst was taken to be 45 m^2/g (from Chapter II) and an exchange current density for oxygen of 5.0×10^{-8} amp/cm^2 was used [23].

4.7 Results and Discussion

The calculated fractional current generation is given in Table 4.1 and the current generation profiles in the electrode layer are shown in Figures 4.5 and 4.6 as functions of catalyst layer thickness and current density. These results agree reasonably well with those obtained from actual operating fuel cells [24,25].

From Figures 4.5 and 4.6 one can see that at low current densities the distribution of the current generation is quite uniform, while at high current densities the majority of the current is generated in that portion of the catalyst-Teflon layer near the electrolyte matrix.

Cell potential and power density are tabulated in Table 4.2, and these are plotted as a function of current density in Figure 4.7. From Figure 4.7 we can see that the limiting current density is approximately 1.3 amp/cm^2, and the maximum power density (0.70 watts/cm^2) is obtained at a current density of about 1.00 amp/cm^2.

It should be noted, however, that in this work it was assumed that there were no gas transport limitations; moreover, it was also assumed that the oxygen contained no impurities which could build up in the gas spaces and introduce gaseous concentration gradients. Thus, the model for which calculations are presented probably overestimates to some degree the proportion of the current generated in the catalyst layer near the electrolyte matrix. Nevertheless, it seems reasonable that at higher current densities most of the current will be

Table 4.1

Fraction of Current Generation in the Electrode Layer.

Current Density amp/cm^2 / Distance from Electrolyte Matrix, cm	0.10	0.20	0.40	0.60	0.80	1.00	1.20
0.001	0.129	0.157	0.211	0.265	0.312	0.356	0.399
0.002	0.118	0.133	0.154	0.167	0.172	0.173	0.171
0.003	0.109	0.115	0.119	0.117	0.113	0.107	0.102
0.004	0.103	0.102	0.098	0.092	0.085	0.079	0.073
0.005	0.098	0.093	0.084	0.076	0.069	0.063	0.057
0.006	0.094	0.087	0.076	0.066	0.059	0.054	0.049
0.007	0.090	0.082	0.069	0.060	0.053	0.047	0.042
0.008	0.088	0.079	0.065	0.055	0.048	0.043	0.038
0.009	0.087	0.077	0.063	0.052	0.046	0.040	0.035
0.010	0.086	0.076	0.062	0.051	0.044	0.039	0.034

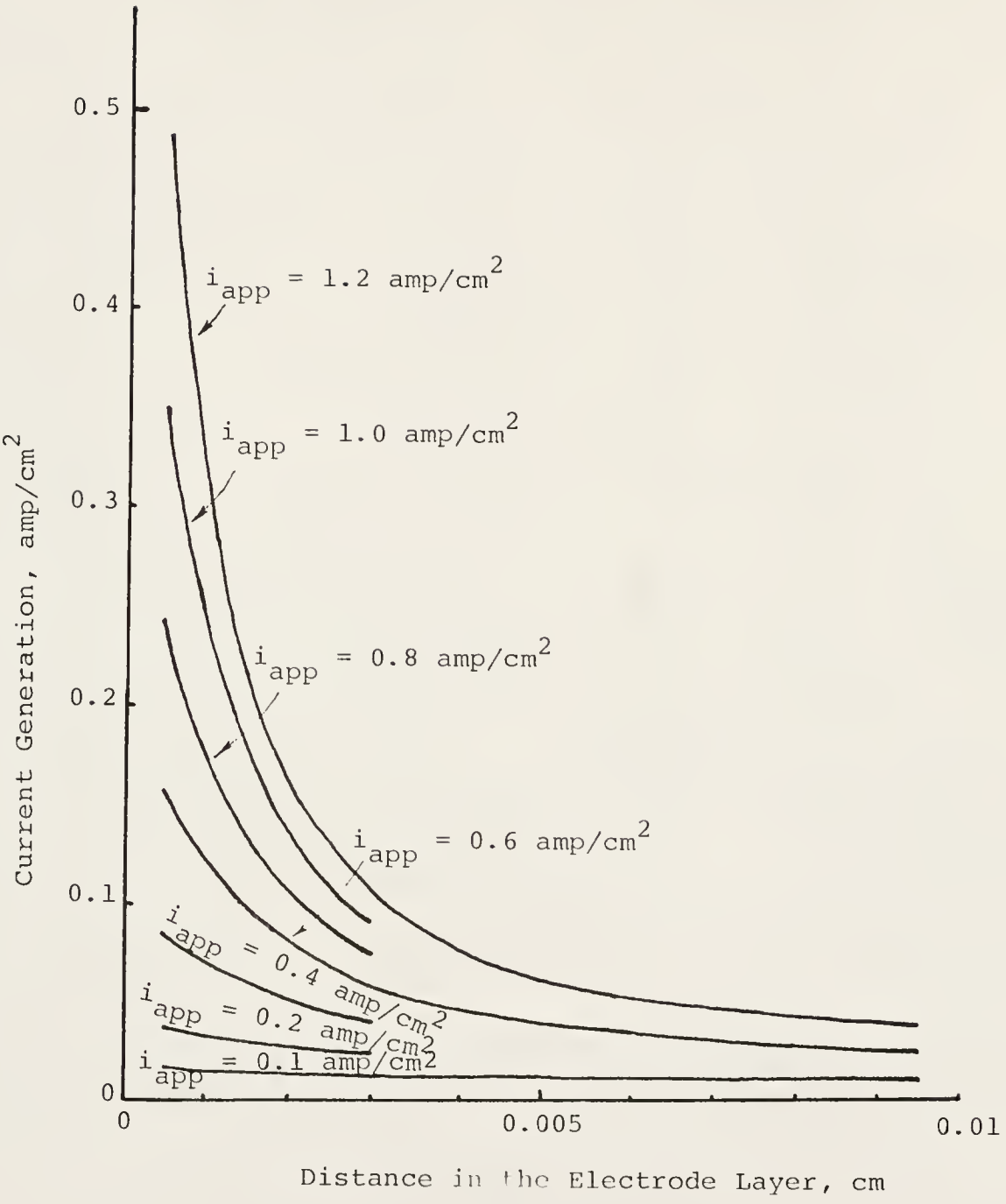

Figure 4.5: Current Generation Distribution in the Electrode Layer.

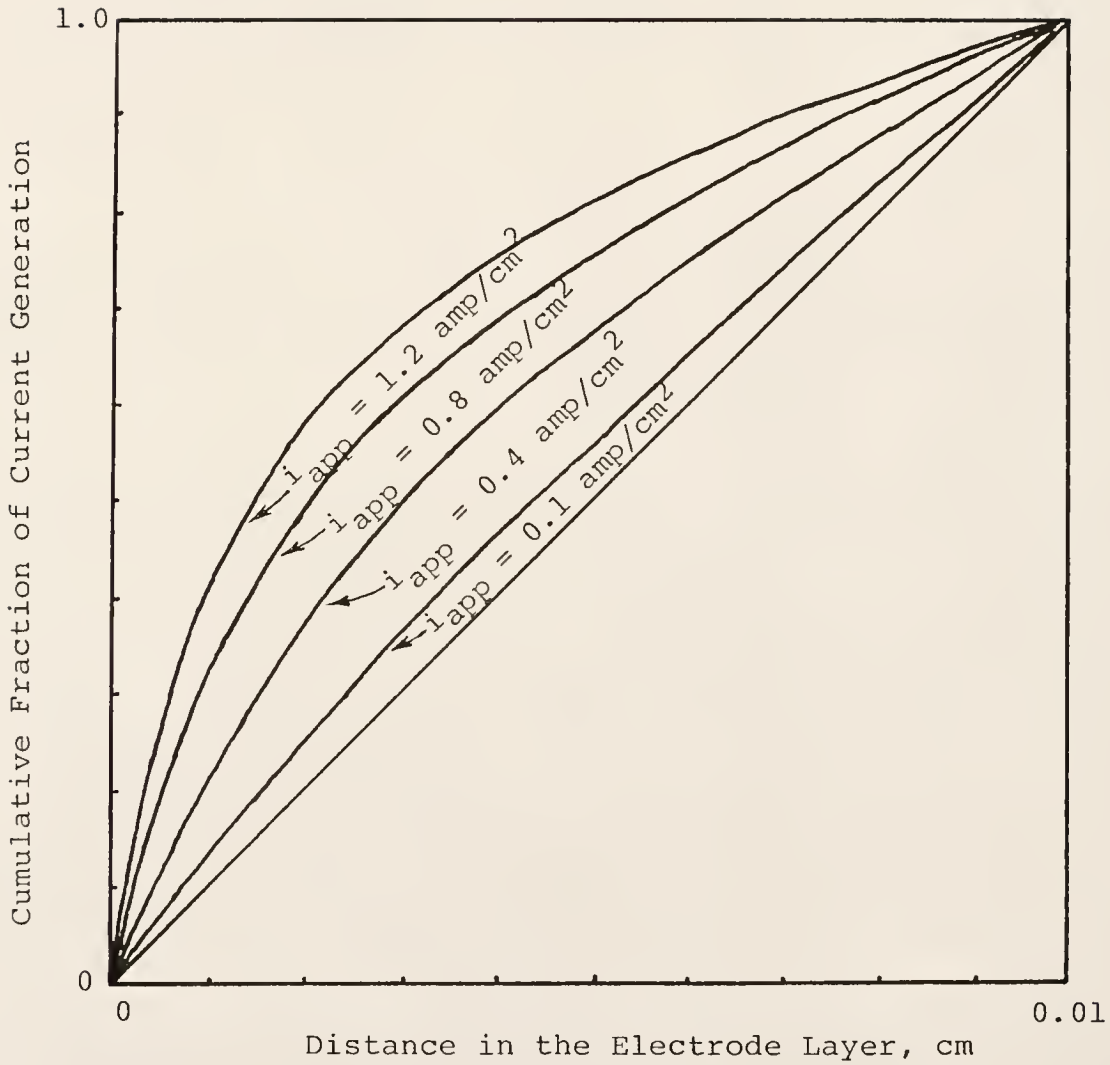

Figure 4.6: Cumulative Fraction of Current Generation in the Electrode Layer.

Table 4.2

Cell Potential and Power Density vs. Current Density.

Current Density, amp/cm^2	Cell Potential, volt	Power, watt/cm^2
0.010	1.085	0.011
0.050	1.058	0.053
0.100	1.039	0.104
0.200	1.009	0.202
0.300	0.979	0.294
0.400	0.948	0.379
0.500	0.914	0.457
0.600	0.878	0.527
0.700	0.841	0.589
0.800	0.802	0.641
0.900	0.762	0.686
1.000	0.704	0.704
1.100	0.631	0.694
1.200	0.489	0.587

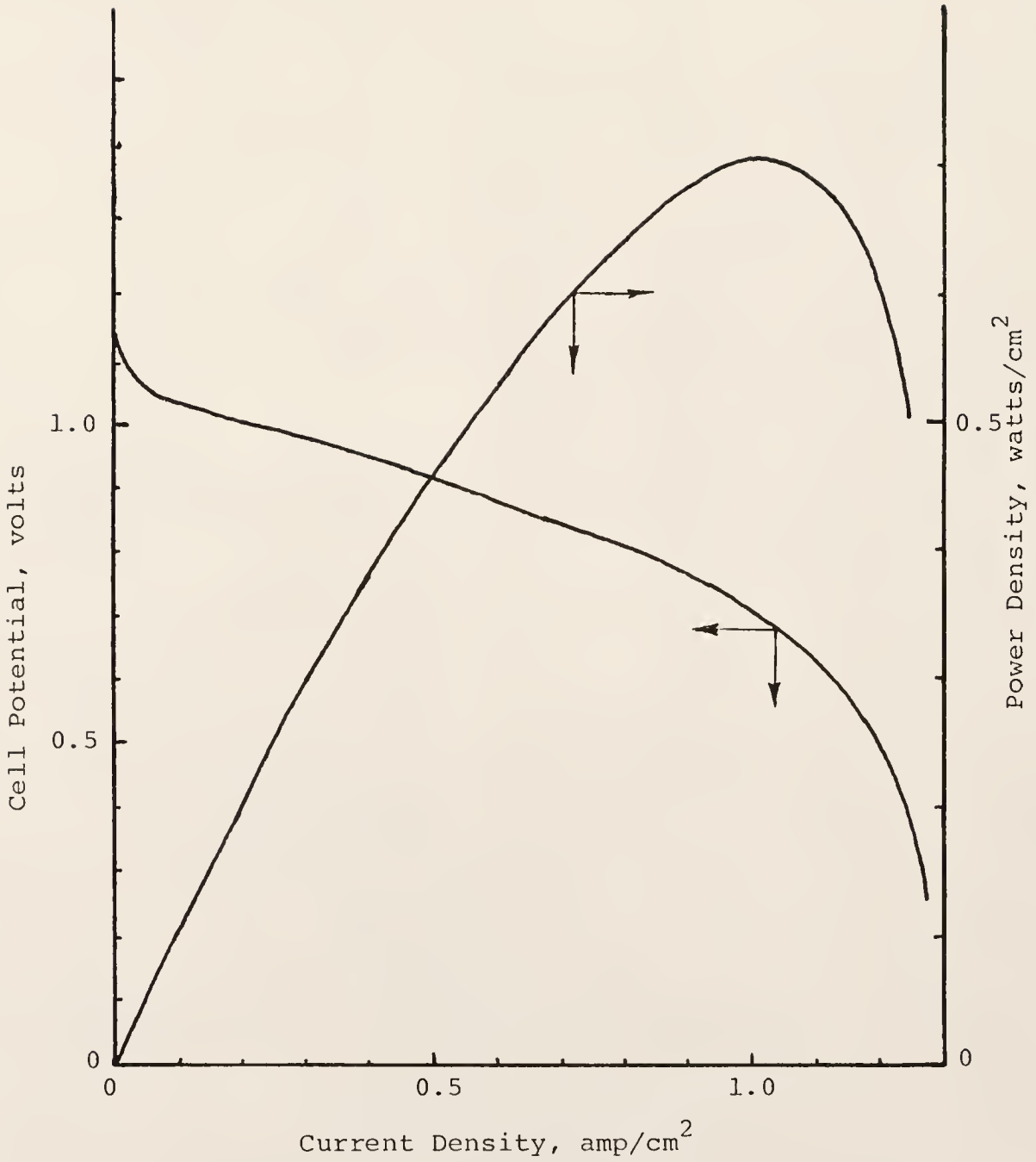

Figure 4.7: Cell Potential and Power Density vs. Current Density.

generated near the electrolyte matrix because of the enormous difference between liquid-phase and gas-phase transport coefficients, and because of the low solubility of oxygen in concentrated KOH.

CHAPTER V

SUMMARY AND CONCLUSION

After a brief description of fuel cells and their performance as these are related to the thermodynamics and kinetics of the electrode reactions, the transport processes occurring in an alkaline hydrogen-oxygen fuel cell are discussed along with the problems associated with the design of electrodes having improved performance. However, the principal studies completed by the author and reported in this dissertation are concerned with: 1) determination of the surface areas of electrode components and evaluation of the effect of processing temperatures on surface areas, 2) estimation of particle sizes and geometry of the components in the electrodes, 3) investigation of the details of the microstructure of fuel cell electrodes by means of scanning electron microscopy and energy dispersive X-ray analysis resulting in the development of a new physical picture of electrode structure, 4) evaluation of the influence of ion hydration on concentration gradients and mass transport, 5) development of a physical and mathematical model for analysis, 6) development of a computer program for use in predicting electrode behavior, and 7) computation and analysis of current generation distribution in the electrode layer.

Surface areas of platinum catalyst, Teflon 30 particles, and their mixtures in different ratios were measured by the BET gas adsorption method; these have been compared with geometrical calculations to provide information as to their sizes and the microstructure of the catalyst-Teflon layer, particularly in relation to the results obtained by scanning electron microscopy. The dependence of surface area of platinum black on the temperature of pretreatment was also measured and related to electrode processing procedures. It was also found that the surface area of the platinum catalyst depends strongly on the pretreatment temperature range of 310 to 350 °C. This finding was very important as the nominal sintering temperature during electrode fabrication is about 310 °C. For example, it was shown that present electrode sintering temperatures are very close to the temperature at which the catalyst itself is sintered, producing a large reduction in surface area. The need for very good temperature control during electrode sintering was demonstrated.

Scanning electron microscopy and energy dispersive X-ray analysis techniques were used in investigating the detailed structure of pure Teflon and catalyst layer of different platinum black-Teflon ratios. This provided information on the size, shape, and microstructure of the catalyst-Teflon layer and on the arrangement and distribution of catalyst and Teflon aggregates. These studies showed, for example, that Teflon 30 particles are aggregates of smaller particles which appear to be Teflon molecules. Separate calculations, based

on the mean molecular weight of the Teflon and its density, conform the conclusions drawn from electron microscopy. The aggregates have a prolate spheroidal shape with minor and major diameters of 1000 to 1500 A (100 to 150 nm) and 2000 to 3000 A (200 to 300 nm), respectively, while the molecules appear to be spheres with diameters ranging from 200 to 300 A (20 to 30 nm). In a commonly used electrode composition of 80:20 platinum black and Teflon, the Teflon aggregates are seen to be coated with one or more layers of catalyst crystallites. This is the exact opposite of the previously held view of the structure of the catalyst-Teflon layer, namely, that this layer consists of roughly spherical agglomerates of catalyst (diameter about one micrometer) surrounded by prolate spheroidal Teflon particles. The substructure of the Teflon particles has not been previously reported.

The size of individual catalyst crystallites could not be determined clearly by scanning electron microscopy owing to the resolution limitations of the technique, but these studies did enable us to determine that the crystallite size was less than 100 A (10 nm). However, this information, combined with that derived from the surface area studies, made it possible to demonstrate that the catalyst crystallite size is almost certainly in the range of 30 to 50 A (3 to 5 nm).

Ion hydration, which has been ignored in previously published work, has been studied. Since water is a reactant

at the oxygen electrode and a product at the hydrogen electrode and since its concentration influences the concentration of electrolyte components, it is reasonable to expect that ion hydration will affect electrode behavior. Indeed, ion hydration was found to have a significant influence on the concentration of "free" water. In this work a primary hydration number of two for both potassium and hydroxyl ions seems reasonable for the KOH concentration used in fuel cells, and this value was used in the calculation of the mathematical modeling equations. Unfortunately, limitations of time made it impossible to examine in detail the influence of ionic hydration in the mathematical modeling; that will be a principal objective of any further research in this area.

Based on the information obtained earlier from the studies on the size and distribution of electrode components and on the structure of electrodes, a schematic model for mathematical analysis was devised to utilize this information in calculating concentration and current generation profiles. A set of modeling equations was developed and computations done. The results were analyzed to provide information on current generation distribution in the electrode layer for different current densities.

The distribution of current generation and the magnitude of the limiting current density given by mathematical modeling of the oxygen electrode show that at higher current densities most of the current is generated in the region near the electrolyte matrix. It is also clear that there is a need to

determine more adequately the effective mass transport properties of the electrode layer and to develop and analyze more realistic models. Considering the fact that the intra-aggregate voids of Teflon particles have very narrow, tortuous, and interconnected gaseous paths and that the electrolyte wets the catalyst layer coated on the surface of the Teflon aggregates, it seems very likely that there could be some hindrance to mass transport of oxygen in the catalyst-Teflon layer. This point should be investigated in future work, as should the influence of impurities in the oxygen system.

APPENDIX 1

DERIVATION OF FLUX EQUATIONS (EQUATIONS (3.3-5) AND (3.3-6))

From Faraday's Law, we have

$$i = F \sum_i z_i N_i$$

$$= F \sum_i z_i C_i v_i \qquad \text{(A.1-1)}$$

Since the solution, as a whole, is electrically neutral, we have

$$\sum_i z_i C_i = 0 \qquad \text{(A.1-2)}$$

Thus Equation (A.1-1) can be written as

$$i = F \sum_i z_i C_i v_i - F \sum_i (z_i C_i) v_o$$

$$= F \sum_i z_i C_i (v_i - v_o) \qquad \text{(A.1-3)}$$

Therefore, for a 1-1 electrolyte such as KOH, we have

$$i = Fz_+C_+ (v_+ - v_o) + Fz_-C_- (v_- - v_o) \qquad \text{(A.1-4)}$$

From Equations (3.3-3) and (3.3-4), we have

$$C_+ \nabla \mu_+ = RT \left[\frac{C_+ C_o}{C_T \mathcal{D}_{o+}} (v_o - v_+) + \frac{C_- C_+}{C_T \mathcal{D}_{+-}} (v_- - v_+) \right] \qquad \text{(3.3-3)}$$

$$C_-\nabla\mu_- = RT\left[\frac{C_-C_o}{C_T\mathcal{D}_{o-}}(v_o - v_-) + \frac{C_-C_+}{C_T\mathcal{D}_{+-}}(v_+ - v_-)\right] \qquad (3.3\text{-}4)$$

Adding the last two equations, we get

$$C_+\nabla\mu_+ + C_-\nabla\mu_- = \frac{RTC_+C_o}{C_T\mathcal{D}_{o+}}(v_o - v_+) + \frac{RTC_-C_o}{C_T\mathcal{D}_{o-}}(v_o - v_-) \qquad (A.1\text{-}5)$$

The electrochemical potential of the electrolyte, μ_e, is given by

$$\mu_e = \nu_+\mu_+ + \nu_-\mu_- \qquad (A.1\text{-}6)$$

The stoichiometric concentration of the electrolyte can be written as

$$C = \frac{C_+}{\nu_+} = \frac{C_-}{\nu_-} \qquad (A.1\text{-}7)$$

Hence

$$C_+\mu_+ + C_-\mu_- = C(\nu_+\mu_+ + \nu_-\mu_-)$$

$$= C\mu_e$$

Therefore, we get

$$C\nabla\mu_e = \frac{RTC_+C_o}{C_T\mathcal{D}_{o+}}(v_o - v_+) + \frac{RTC_-C_o}{C_T\mathcal{D}_{o-}}(v_o - v_-) \qquad (A.1\text{-}8)$$

Eliminating v_+ from Equations (A.1-4) and (A.1-8), we get

$$\frac{RTC_+C_o i}{C_T\mathcal{D}_{o+}} + Fz_+C_+C\nabla\mu_e$$

$$= \frac{RTC_+C_o}{C_T\mathcal{D}_{o+}}Fz_-C_-(v_- - v_o) + \frac{RTC_-C_o}{C_T\mathcal{D}_{o-}}Fz_+C_+(v_o - v_-)$$

$$= \frac{RTC_o C_+ C_- F}{C_T} \left(\frac{z_+}{\mathcal{D}_{o+}} - \frac{z_-}{\mathcal{D}_{o-}} \right) (v_o - v_-)$$

$$= \frac{RTC_o C_+ C_- F}{C_T} \left(\frac{z_+ \mathcal{D}_{o+} - z_- \mathcal{D}_{o-}}{\mathcal{D}_{o+} \mathcal{D}_{o-}} \right) (v_o - v_-) \qquad \text{(A.1-9)}$$

Therefore

$$C_-(v_o - v_-) = \frac{iz_- \mathcal{D}_{o-}}{z_- F(z_+ \mathcal{D}_{o+} - z_- \mathcal{D}_{o-}} + \frac{C_T C \nabla \mu_e z_+ \mathcal{D}_{o+} \mathcal{D}_{o-}}{RTC_o (z_+ \mathcal{D}_{o+} - z_- \mathcal{D}_{o-})} \qquad \text{(A.1-10)}$$

Substituting Equations (3.3-7) and (3.3-8) into Equations (A.1-10) we get

$$C_-(v_o - v_-) = - \frac{it_-}{z_- F} + \frac{C_T C \nabla \mu_e}{RTC_o} \frac{z_+}{(z_+ - z_-)} \mathcal{D} \qquad \text{(A.1-11)}$$

Since the solution is electrically neutral

$$z_+ C_+ + z_- C_- = 0$$

$$z_+ = - \frac{z_- C_-}{C_+}$$

Hence

$$\frac{z_+}{z_+ - z_-} = \frac{- \frac{z_- C_-}{C_+}}{- \frac{z_- C_-}{C_+} - z_-}$$

$$= \frac{C_-}{C_+ + C_-}$$

$$= \frac{\nu_- C}{\nu_+ C + \nu_- C}$$

$$= \frac{\nu_-}{\nu_+ + \nu_-}$$

$$= \frac{\nu_-}{\nu} \qquad \text{(A.1-12)}$$

Substituting Equation (A.1-12) into Equation (A.1-11), we get

$$C_-(v_o - v_-) = - \frac{it_-}{z_-F} + \frac{C_T C \nabla \mu_e \nu_-}{\nu RTC_o} \mathcal{D} \qquad \text{(A.1-13)}$$

Hence

$$C_- v_- = - \frac{\nu_- \mathcal{D} C_T}{\nu RTC_o} C \nabla \mu_e + \frac{it_-}{z_-F} + C_- v_o \qquad \text{(3.3-6)}$$

Similarly, it can be shown that

$$C_+ v_+ = - \frac{\nu_+ \mathcal{D} C_T}{\nu RTC_o} C \nabla \mu_e + \frac{it_+}{z_+F} + C_+ v_o \qquad \text{(3.3-5)}$$

APPENDIX 2

DERIVATION OF EQUATION (3.3-10)

The electrochemical potential of the electrolyte is given by

$$\mu_e = \nu RT \ell n (C f_{\pm} a_{\pm}^{\theta}) \qquad \text{(A.2-1)}$$

where $f_{\pm}$ is the mean molar activity coefficient of the electrolyte and $a_{\pm}^{\theta}$ is a proportionality constant. The gradient of the electrochemical potential of the electrolyte is then give by

$$\begin{aligned} \nabla \mu_e &= \nu RT \frac{\partial}{\partial x} \ell n (C f_{\pm} a_{\pm}^{\theta}) \\ &= \frac{\nu RT}{C f_{\pm} a_{\pm}^{\theta}} \left(f_{\pm} a_{\pm} \frac{\partial C}{\partial x} + C a_{\pm}^{\theta} \frac{\partial f_{\pm}}{\partial x} \right. \\ &= \frac{\nu RT}{C f_{\pm}} \left(f_{\pm} + C \frac{\partial f_{\pm}}{\partial C} \right) \nabla C \end{aligned} \qquad \text{(A.2-2)}$$

Therefore

$$\begin{aligned} \frac{C \nabla \mu_e}{\nu RT} &= \left(1 + \frac{C \partial f_{\pm}}{f_{\pm} \partial C} \right) \nabla C \\ &= \left(1 + \frac{\partial \ell n f_{\pm}}{\partial \ell n C} \right) \nabla C \end{aligned}$$

Thus

$$\frac{\mathcal{D} C_T}{\nu RT C_o} C \nabla \mu_e = \left(\frac{\mathcal{D} C_T}{C_o} \right) \left(1 + \frac{d \ell n f_{\pm}}{d \ell n C} \right) \nabla C \qquad \text{(A.2-3)}$$

The measured diffusion coefficient of the electrolyte, D, is related to $\mathcal{D}$ by

$$D = \mathcal{D}(1 + \nu M_o m)\left(1 + \frac{d\ell n\gamma_{\pm}}{d\ell nm}\right) \qquad (A.2\text{-}4)$$

$\therefore$

$$\nu = \nu_+ + \nu_-$$

$$m = \frac{C}{\rho - \sum_{j=0} C_j M_j} = \frac{C}{C_o M_o} \qquad (A.2\text{-}5)$$

Therefore

$$D = \mathcal{D}\left(1 + (\nu_+ + \nu_-)\, M_o \frac{C}{C_o M_o} \right)\left(1 + \frac{d\ell n\gamma_{\pm}}{d\ell nm} \right)$$

$$= \mathcal{D}\left(\frac{C_o + C_+ + C_-}{C_o} \right)\left(1 + \frac{d\ell n\gamma_{\pm}}{d\ell nm} \right)$$

$$= \mathcal{D}\,\frac{C_T}{C_o}\left(1 + \frac{d\ell n\gamma_{\pm}}{d\ell nm} \right) \qquad (A.2\text{-}6)$$

Hence we get

$$\frac{\mathcal{D}C_T}{\nu RTC_o}\, C\nabla\mu_e = \frac{D\left(1 + \frac{d\ell nf_{\pm}}{d\ell nC} \right)}{\left(1 + \frac{d\ell n\gamma_{\pm}}{d\ell nm} \right)}\nabla C \qquad (A.2\text{-}7)$$

The measured diffusion coefficient of the electrolyte, D, is also related to $\mathcal{D}$ by the following relation

$$D = \frac{\mathcal{D}\,\frac{1 + \nu M_o m}{1 + Mm}\left(1 + \frac{d\ell nf_{\pm}}{d\ell nC} \right)}{\left(1 - \frac{d\ell n\rho}{d\ell nC} \right)} \qquad (A.2\text{-}8)$$

From Equations (A.2-4) and (A.2-8), we get

$$\frac{1 + \frac{d\ell nf_{\pm}}{d\ell nC}}{1 + \frac{d\ell n\gamma_{\pm}}{d\ell nm}} = (1 + Mm)\ (1 - \frac{d\ell n\rho}{d\ell nC})$$

$$= \left(1 + \frac{MC}{C_o M_o} \right) \left(1 - \frac{d\ell n\rho}{d\ell nC} \right)$$

$$= 1 + \frac{MC}{C_o M_o} - \left(1 + \frac{MC}{\rho_o} \right) \frac{d\ell n\rho}{d\ell nC}$$

$$= 1 + \frac{MC}{C_o M_o} - \frac{\rho d\ell n\rho}{\rho_o d\ell nC}$$

$$= 1 - \left(\frac{\rho d\ell n\rho}{\rho_o d\ell nC} - \frac{MC}{\rho_o} \right) \qquad \text{(A.2-9)}$$

$$\therefore \quad \rho = C_o M_o + MC$$

$$\frac{d\ell n\rho}{dC} = \frac{1}{C_o M_o + MC} \frac{\partial}{\partial C} (C_o M_o + MC)$$

$$= \frac{1}{\rho} M_o \frac{\partial C_o}{\partial C} + \frac{M}{\rho}$$

Multiplying each side of the above equation by C, we get

$$\frac{d\ell n\rho}{d\ell nC} = \frac{C}{\rho} M_o \frac{\partial C_o}{\partial C} + \frac{MC}{\rho}$$

$$= \frac{C\rho_o \partial C_o}{C_o \rho \partial C} + \frac{MC}{\rho}$$

$$= \frac{\rho_o \ell nC_o}{\rho \ell nC} + \frac{MC}{\rho} \qquad \text{(A.2-10)}$$

Substituting Equation (A.2-10) into Equation (A.2-9), we get

$$\frac{1 + \frac{d\ell nf_{\pm}}{d\ell nC}}{1 + \frac{d\ell n\gamma_{\pm}}{d\ell nm}} = 1 - \left(\frac{\rho}{\rho_o} \left(\frac{\rho_o d\ell nC_o}{\rho\ d\ell nC} + \frac{MC}{\rho} \right) - \frac{MC}{\rho_o} \right)$$

$$= 1 - \left(\frac{d\ell nC_o}{d\ell nC} + \frac{MC}{\rho_o} - \frac{MC}{\rho_o} \right)$$

$$= 1 - \frac{d\ell nC_o}{d\ell nC} \qquad \text{(A.2-11)}$$

Substituting Equation (A.2-11) into Equation (A.2-7), we thus get

$$\frac{C_T}{\nu RTC_o} C\nabla\mu_e = D \left(1 - \frac{d\ell nC_o}{d\ell nC} \right) \nabla C \qquad \text{(3.3-10)}$$

APPENDIX 3

CONVERSION OF D^V TO D*
(VOLUME AVERAGE FRAME DIFFUSIVITY TO MOLAR AVERAGE FRAME DIFFUSIVITY)

Since the diffusion data that we have on KOH from Bhatia are in the volume average frame only, they have to be transformed into the molar average frame to be used in our equations. The diffusion flux in the volume average frame can be related to that in the molar average frame in the following manner. For a binary system, from the definition of volume average frame,

$$v^V = \rho_A v_A \frac{\bar{V}_A}{M_A} + \rho_B v_B \frac{\bar{V}_B}{M_B} \qquad \text{(A.3-1)}$$

$$j_A^V = \rho_A (v_A - v^V) \qquad \text{(A.3-2)}$$

Substitution of Equation (A.3-1) into Equation (A.3-2) gives

$$j_A^V = \rho_A \left[v_A - \left(\rho_A v_A \frac{\bar{V}_A}{M_A} + \rho_B v_B \frac{\bar{V}_B}{M_B} \right) \right]$$

$$= \rho_A \left[v_A - (C_A v_A \bar{V}_A + C_V v_B \bar{V}_B) \right]$$

$$= \rho_A v_A (1 - C_A \bar{V}_A) - \rho_A C_B v_B \bar{V}_B \qquad \text{(A.3-3)}$$

Dividing Equation (A.3-3) by M_A gives

$$J_A^V = C_A v_A (1 - C_A \bar{V}_A) - C_A C_B v_B \bar{V}_B \qquad \text{(A.3-4)}$$

Since $N_A = C_A v_A = J_A^* + C_A v^*$,

$N_B = C_B v_B = J_B^* + C_B v^*$,

and $C_A \bar{V}_A + C_B \bar{V}_B = 1$,

Equation (A.3-4) becomes

$$\begin{aligned} J_A^V &= (J_A^* + C_A v^*)\ C_B \bar{V}_B - (J_B^* + C_B v^*)\ C_A \bar{V}_B \\ &= (C_B J_A^* + C_A C_B v^* - C_A J_B^* - C_A C_B v^*)\ \bar{V}_B \\ &= (C_B J_A^* - C_A J_B^*)\ \bar{V}_B \end{aligned} \qquad \text{(A.3-5)}$$

Since $J_A^* + J_B^* = 0$, Equation (A.3-5) becomes

$$J_A^V = J_A^*\ (C_A + C_B)\ \bar{V}_B \qquad \text{(A.3-6)}$$

Since $J_A^V = -D^V \nabla C_A$ and $J_A^* = -D^* \nabla C_A$, (A.3-6) becomes $-D^V \nabla C_A = -D^*\ (C_A + C_B)\ \bar{V}_B \nabla C_A$. Therefore, $D^* = \dfrac{D^V}{(C_A + C_B)\bar{V}_B}$.

APPENDIX 4

CALCULATION OF $C_3(r,x)$ FOR A GIVEN x

The flux equation for C_3 is [26]

$$D_3 \frac{d^2C_3}{dr^2} + \frac{D_3}{r}\frac{dC_3}{dr} - \frac{1}{RF}\frac{di_s}{dx} = 0 \qquad \text{(A.4-1)}$$

Substitution of Equation (5.1-1) into Equation (A.4-1) gives

$$D_3 \frac{d^2C_3}{dr^2} + \frac{D_3}{r}\frac{dC_3}{dr} - C_3\left[\frac{\alpha i_o}{nFC_3}\left(\frac{C_4(x)}{C_4^o}\right)\exp\left(-\frac{F(\phi_s-\phi_\ell)}{RT}\right) - \frac{\alpha i_o}{nF}\left(\frac{C_1(x)}{C_1^o}\right)\exp\left(\frac{F(\phi_s-\phi_\ell)}{RT}\right)\right] = 0 \qquad \text{(A.4-2)}$$

Let

$$q^2 = \frac{\alpha i_o}{nFC_3^oD_3}\frac{C_4(x)}{C_4^o}\exp\left(-\frac{F(\phi_s-\phi_\ell)}{RT}\right) \qquad \text{(A.4-3)}$$

and

$$C_3' = C_3 - C_3^o\left[\frac{C_1(x)\ C_4^o}{C_1^o\ C_4(x)}\exp\left(\frac{2F(\phi_s-\phi_\ell)}{RT}\right)\right] \qquad \text{(A.4-4)}$$

Then Equation (A.4-2) becomes

$$\frac{d^2C_3'}{dr^2} + \frac{1}{r}\frac{dC_3'}{dr} - q^2C_3' = 0 \qquad \text{(A.4-5)}$$

The following boundary conditions can be used in solving Equation (A.4-5),

B.C.1: At $r=r_o$, $C_3' = C_3^e - C_3^o\left(\frac{C_1(x)}{C_1^o}\frac{C_4^o}{C_4(x)}\right)\exp\left(\frac{2F(\phi_s-\phi_\ell)}{RT}\right)$

$= C_o'$

where C_3^e is the equilibrized concentration at the gas-electrolyte interface.

B.C.2: At $r=r_o+\delta$, $\frac{dC_3'}{dr} = 0$

The solution to Equation (A.4-5) is

$$C_3' = A_1 I_o(qr) + A_2 K_o(qr) \qquad \text{(A.4-6)}$$

where A_1 and A_2 are constants and $I_o(qr)$ and $K_o(qr)$ are Bessel functions of zero order. Applying B.C.'s, we have

$$\text{at } r=r_o, \quad C_o' = B_1 I_o(qr_o) + B_2 K_o(qr_o) \qquad \text{(A.4-7)}$$

$$\text{at } r=r_o+\delta, \quad 0 = B_1 I_1(q(r_o+\delta)) + B_2 K_1(q(r_o+\delta)) \qquad \text{(A.4-8)}$$

From Equations (A.4-7) and (A.4-8) we have

$$A_1 = \frac{C_o' K_1(q(r_o+\delta))}{K_1(q(r_o+\delta))I_o(qr_o) + K_o(qr_o)I_1(q(r_o+\delta))}$$

and

$$A_2 = \frac{C_o K_1(q(r_o+\delta))}{K_1(q(r_o+\delta))I_o(qr_o) + K_o(qr_o)I_1(q(r_o+\delta))}$$

Substituting these into Equation (A.4-6) gives

$$C_3' = \frac{C_o'}{K_1(q(r_o+\delta))I_o(qr_o) + K_o(qr_o)I_1(q(r_o+\delta))} \times$$

$$[K_1(q(r_o+\delta))I_o(qr) + I_1(q(r_o+\delta))K_o(qr)] \qquad \text{(A.4-9)}$$

or

$$C_3 - C_3^o \frac{C_1(x)\ C_4^o}{C_1^o\ C_4(x)} \exp \frac{2F(\phi_s-\phi_\ell)}{RT} = \frac{C_3^e - C_3^o \frac{C_1(x)\ C_4^o}{C_1^o\ C_4(x)} \exp \frac{2F(\phi_s-\phi_\ell)}{RT}}{DEN} \times$$

$$[K_1(q(r_o+\delta))I_o(qr) + I_1(q(r_o+\delta))K_o(qr)] \qquad \text{(A.4-10)}$$

where $DEN = K_1(q(r_o+\delta))I_o(qr_o) + K_o(qr_o)I_1(q(r_o+\delta))$.

Dividing Equation (A.4-10) by C_3^o gives

$$\frac{C_3}{C_3^o} = \frac{C_1(x)\ C_4^o}{C_1^o\ C_4(x)} \exp \frac{2F(\phi_s-\phi_\ell)}{RT} + \left(\frac{C_3^e}{C_3^o} - \frac{C_1(x)\ C_4^o}{C_1^o\ C_4(x)} \exp\left(\frac{2F(\phi_s-\phi_\ell)}{RT}\right)\right) \times$$

$$\frac{[K_1(q(r_o+\delta))I_o(qr) + I_1(q(r_o+\delta))K_o(qr)]}{DEN} \qquad \text{(A.4-11)}$$

Taking the average using

$$\bar{C}_3(x) = \int \frac{2\pi r C_3(r,x)}{\pi r^2}\, dr$$

gives

$$\frac{\bar{C}_3(x)}{C_3^o} = \frac{C_1(x)\ C_4^o}{C_1^o\ C_4(x)} \exp\left(\frac{2F(\phi_s-\phi_\ell)}{RT}\right) + \frac{2r_o}{q(DEN)} \left(1 - \frac{C_1(x)\ C_4^o}{C_1^o\ C_4(x)} \times \exp\left(\frac{2F(\phi_s-\phi_\ell)}{RT}\right)\right) \frac{[I_1(q(r_o+\delta))K_1(qr_o) - K_1(q(r_o+\delta))I_1(qr_o)]}{2r_o\delta + \delta^2}$$

(4.5-2)

With this average value of $\frac{\bar{C}_3(x)}{C_3}$, Equation (5.1-1) becomes

$$\frac{di_s}{dx} = \alpha i_o \left[\frac{\bar{C}_3(x)}{C_3^o} \frac{C_4(x)}{C_4^o} \exp\left(- \frac{F(\phi_1 - \phi_\ell)}{RT} \right) - \frac{C_1(x)}{C_1} \exp\left(\frac{F(\phi_s - \phi_\ell)}{RT} \right) \right] \tag{4.5-3}$$

APPENDIX 5

COMPUTER PROGRAMMING FOR THE COMPUTATION OF CURRENT DENSITY DISTRIBUTION

The computer programming for the computation of current density distribution is listed below:

```
C
C
C
C
C     MATHEMATICAL MODELLING OF A FUEL CELL ELECTRODE
C
      DIMENSION  CKOH(20), CH2O(20), PHI(20), PHS(20)
      DIMENSION  CURCAT(20), DLCRCT(20), POS(20), CONY(20)
      REAL   K1, K2, K3, K4
      ------------------------------------------------------------
C
C
C     VARIATION OF THE WITHDRAWING CURRENT
C
      JN = 12
      DO  300  J = 1, JN
      CURAPP = 0.100 * J
      CURCAT(1) = 0.0
      PHIASS = 0.50 + 0.035 * J
      DELTPH = 0.05
      LN = 10
  111 DO  400  I = 1, LN
      PHIASS = PHIASS - DELTPH
      PHI(1) = PHIASS
      PHS(1) = 0.0
      DLPHSL = PHS(1) - PHI(1)
      CKOH(1) = 6.7979
C
C     NUMERICAL INTEGRATION
C
      N = 32
      THICK = 0.01
      WIDTH = THICK / N
C
      DO  100  I = 1, N
      ARG1 = 38.84 * DLPHSL
      ARG2 = ARG1 * 2.0
      POS(I) = WIDTH * I
      AA = ( CURAPP - CURCAT(I) ) * 259.0
      CNKOH = CKOH(I)
C
C     PARTIAL MOLAL VOLUME OF WATER
C
      PARV4 = 0.0182297 + CNKOH * ( 7.37463*10.**(-5) -
     C          CNKOH * ( 4.76316*10.**(-5) - CNKOH * ( 4.67409
     C          *10.**(-6) - 1.65384*10.**(-7) * CNKOH )))
C
C     CONCENTRATION OF WATER
C
      CH2O(I) = 54.7356 - CNKOH * ( 4.5103 + CNKOH * ( 5.1709*
     C          10.**(-2) - 1.243*10.**(-3) * CNKOH ))
      CNH2O = CH2O(I)
```

```
C
C   PARTIAL MOLAL VOLUME OF KOH
C
      PARV = ( 1.00 - CNH2O * PARV4) / CNKOH
C
      DCOVDX = AA * ( 1.0 - CNKOH*PARV ) * ( 1.0 - CNKOH *
     C          ( PARV - PARV4 )) / ( 1.0 - CNKOH * PARV +
     C          2.0 * CNKOH * PARV4 )
C
      G = SQRT ( 1.74143 * CNH2O * EXP(-ARG1) )
C
      R1 = G * 1.00 * 10.**(-5)
      R2 = G * 1.04 * 10.** (-5)
C
      CALL   FE03A ( BSLI0,  BSLK0,  R1, 2 )
      CALL   FE04A ( BSLI11, BSLK11, R1, 2 )
      CALL   FE04A ( BSLI12, BSLK12, R2, 2 )
C
      DNU = BSLI12 * BSLK11 - BSLK12 * BSLI11
      DEN = BSLK12 * BSLI0 + BSLK0 * BSLI12
C
      CNOXY(I) = 0.0001981 * ( ( CNKOH/CNH2O ) * EXP(ARG2)
     C          + 2.451*10.**(6) * ( 1.0 - 5.248 * ( CNKOH
     C          /CNH2O ) * EXP(ARG2) ) * DNU / ( G * DEN ) )
      CNOXY = CNOXY(I)
C
C   CONDUCTIVITY OF ELECTROLYTE
C
      CONDUC = -0.55876 + CNKOH * ( 0.608757 - CNKOH *
     C          ( 0.0688246 - 0.00229369 * CNKOH ) )
C
      DIADIC = CNKOH * ( 1621.34374 * CNKOH - 8626.2874 ) /
     C          ( 21903.605 - CNKOH * ( 8626.2874 - 810.67187
     C          * CNKOH ) )
C
      DELPHI = ( ( CURCAT(I) - CURAPP ) / CONDUC - ( 0.05741
     C          / CNKOH ) * ( 0.924 + 2.5 * CNKOH/CNH2O ) *
     C          DCOVDX * DIADIC ) * WIDTH
      PHL(I+1) = PHL(I) + DELPHI
C
      ALPHA = 4.50 * 10.**(+5)
      XCHGRD = 5.0 * 10.**(-8)
C
C   CURRENT GENERATION
C
      DLCRCT(I) = ALPHA * XCHGRD * ( 0.7425 * CNOXY * CNH2O
     C          * EXP(-ARG1) - ( CNKOH/6.7979 ) *
     C          EXP(ARG1) ) * WIDTH
      CURCAT(I+1) = CURCAT(I) + DLCRCT(I)
C
      RHO = 1000
      DELPHS = (-CURCAT(I+1) / RHO ) * WIDTH
      PHS(I+1) = PHS(I) + DELPHS
      DLPHSL = PHS(I+1) - PHL(I+1)
C
C   CALCULATION OF KOH CONCENTRATION BY THE
C   QUADRATIC RUNGE-KUTTA METHOD
C
      BB = WIDTH * AA
C
      K1 = BB * ( 1.0 - CNKOH*PARV ) * ( 1.0 - CNKOH * (
     C     PARV - PARV4 ) ) / ( 1.0 - CNKOH*( PARV - 2.0 *
     C     PARV4 ) )
C
      K2 = BB * ( 1.0 - ( CNKOH + (1/2.0 ) * PARV ) * ( 1.0
     C     - ( CNKOH + K1/2.0 ) * ( PARV - PARV4 ) ) / ( 1.0 -
     C     ( CNKOH + K1/2.0 ) * ( PARV - 2.0 * PARV4 ) )
```

```
      K3 = BB * ( 1.0 - ( CNKOH + K2/2.0 ) * PARV ) * ( 1.0 -
     C      ( CNKOH + K2/2.0 ) * ( PARV - PARV4 ) ) / ( 1.0 -
     C      ( CNKOH + K2/2.0 ) * ( PARV - 2.0 * PARV4 ) )
C
      K4 = BB * ( 1.0 - ( CNKOH + K3 ) * PARV ) * ( 1.0 -
     C      ( CNKOH + K3 ) * ( PARV - PARV4 ) ) / ( 1.0 -
     C      ( CNKOH + K3 ) * ( PARV - 2.0 * PARV4 ) )
C
      DLCKOH = ( K1 + 2.0 * K2 + 2.0 * K3 + K4 ) / 6.0
      CKOH(I+1) = CKOH(I) + DLCKOH
      IF ( CURCAT(I+1).GT.CURAPP .AND. I.LT.N ) GO TO 400
  100 CONTINUE
C
      ACC = CURAPP * 0.025
      IF ( ABS(CURCAT(N+1)-CURAPP) - ACC ) 200, 200, 112
  112 PHLASS = PHLASS + DELTPH
      DELTPH = DELTPH/LN
      IF ( DELTPH .LT. 0.000004 ) GO TO 200
      GO TO 111
  400 CONTINUE
C
  200 WRITE (6, 101)  CURAPP
  101 FORMAT ('1', 5X, 'CURRENT WITHDRAWN FROM THE SYSTEM =',
     C          F10.5, ////)
      WRITE (6, 102)
  102 FORMAT (9X, 'LOCATION', 3X, 'CONCN OF KOH', 3X,
     C        'CONCN OF WATER', 2X, 'ELECTROLYTE POT', 2X,
     C        'CATALYST POT', 5X, 'CURR  GENERN', 6X,
     C        'CURR IN CAT', // )
C     ------------------------------------------------------------------
      DO  500  M = 1, N
      WRITE (6, 103) POS(M), CKOH(M), CH2O(M), PHL(M),
     C                PHS(M), DLCRCT(M), CURCAT(M+1)
  103 FORMAT ( F17.5, 6F16.5,  / )
  500 CONTINUE

  300 CONTINUE
      STOP
      END


      SUBROUTINE FF03A(VIS,VKS,S,N)
      REAL * 8 A(19)    /
     1     .1D-19                          , .42D-18                      ,
     2     .3132D-16                       , .206305D-14                  ,
     3     .11989083D-12                   , .60968928D-11                ,
     4     .26882812895D-9                 , .1016972672769D-7            ,
     5     .32609105057896D-6              , .873831549662236D-5          ,
     6     .19246935963811366D-3           , .34163317660123410D-2        ,
     7     .47718748798174135D-1           , .50949336543998287D0         ,
     8     .40116737601793485D1            , .22274819242462231D2         ,
     9     .82489032744024099D2            , .19049432017274284D3         ,
     A     .25546687962436217D3            /
      REAL * 8 B(19)    /
     A     .1D-19                          , .63D-18                      ,
     B     .4523D-16                       , .285752D-14                  ,
     C     .15855413D-12                   , .765757438D-11               ,
     D     .31858797963D-9                 , .112812113876D-7             ,
     E     .33519525563133D-6              , .821602593993066D-5          ,
     F     .16270837904302330D-3           , .25363081880861990D-2        ,
     G     .30080722420511874D-1           , .259084432434900197D0        ,
     H     .15115356760292279D1            , .528363286687392001D1        ,
     I     .80053688697003348D1            ,-.456343358644839 5D1         ,
     J    -.21057660177402440D2            /
      REAL * 8 C(26)    /
     J     .1D-13                          , .2D-13                       ,
     J     .0D-13                          ,-.4D-13                       ,
     K    -.11D-12                         ,-.11D-12                      ,
```

```
L      .12D-12                    , .7D-12                    ,
M      .14D-11                    , .111D-11                  ,
N     -.245D-11                   ,-.1223D-10                 ,
O     -.2896D-10                  ,-.4361D-10                 ,
P     -.1954D-10                  , .15142D-9                 ,
Q      .78081D-9                  , .287935D-8                ,
R      .1045317D-7                , .4342656D-7               ,
S      .227083D-6                 , .157817791D-5             ,
T      .1527877872D-4             , .22510873571D-3           ,
U      .6278240302740-2           , .79833170337777D0         /
      REAL*8 X1,X2,X3,X4,VI0,VK0,X,Y,Z,Q1,Q2,Q3,FX,XD
      REAL * 8 XLG/77FFFFFFFFFFFFFFFF/
      EQUIVALENCE(A(20),B(1)),(B(20),C(1))
      IENT=1
      X=DBLE(S)
      GO TO 44
      ENTRY FF03AD(VI0,VK0,XD,N)
      IENT=2
      X=XD
   44 Y=DABS(X)
      Z=Y*.125D0
      IF(Z .GT. 1D0)GO TO 42
      IF(Z .LE. 0D0)GO TO 78
      X2=4D0*Z*Z-2D0
      JUMP=1
      N1=1
      N2=19
   70 Q3=0D0
      Q2=0D0
      DO 40 I=N1,N2
      Q1=Q2
      Q2=Q3
      Q3=X2*Q2-Q1+A(I)
   40 CONTINUE
      FX=(Q3-Q1)*.5D0
      GO TO (50,51,52,53),JUMP
   50 VI0=FX
      IF(IENT.EQ.1)VIS=SNGL(VI0)
      IF(N.LE.0)GO TO 75
      JUMP=2
      N1=20
      N2=38
      GO TO 70
   78 VK0=XLG
      VI0=1D0
      IF(IENT .EQ.2)GO TO 75
      VKS=XLG
      VIS=1E0
      GO TO 75
   51 VK0=-DLOG(Z)*VI0+FX
      IF(IENT.EQ.1)VKS=SNGL(VK0)
   75 RETURN
   42 Z=1D0/Z
      X2=Z+Z
      JUMP=3
      N1=39
      N2=64
      X1=1D0/DSQRT(Y)
      X3=DEXP(Y)
      IF(N-1)70,100,70
   52 VI0=X3*FX*X1
      IF(IENT.EQ.1)VIS=SNGL(VI0)
  100 IF(N.EQ.0)GO TO 75
  101 JUMP=4
      X2=-Z-Z
      GO TO 70
   53 VK0=3.14159265358979 3D0*X1*FX/X3
      IF(IENT.EQ.1)VKS=SNGL(VK0)
      GO TO 75
      END
```

```
      SUBROUTINE FF04A(VIS,VKS,S,N)
      REAL * 8 A(18)   /
     1      .9D-19                          , .718D-17                  ,
     2      .50120D-15                      , .3095296D-13              ,
     3      .1675972820-11                  , .7929055929D-10           ,
     4      .3227616520230-8                , .1119462845638 9D-6       ,
     5      .3264138122309860-5             , .7875678575416515D-4      ,
     6      .1543019015627219 1D-2          , .2399307914784055 2D-1    ,
     7      .2878555118046720 3D0           , .2571459906347754 9D1     ,
     8      .1633455055252206 6D2           , .6939591763373444 8D2     ,
     9      .1813126160405702 7D3           , .2598902378064772 9D3     /
      REAL * 8 B(18)   /
     A      .14D-18                         , .1057D-16                 ,
     B      .70860D-15                      , .4187279D-13              ,
     C      .216255319D-11                  , .96659752D-10             ,
     D      .369678327836D-8                , .11936797074664D-6        ,
     E      .320251069193505D-5             , .70010627854757 53D-4     ,
     F      .121705699451574 09D-2          , .16300049289816418D-1     ,
     G      .161074301656147 82D0           , .11014619930048522D1      ,
     H      .466638702686284 19D1           , .93616178313953887D1      ,
     I     -.183923922428619 94D1           ,-.26688095480862668D2      /
      REAL * 8 C(26)   /
     J     -.1D-13                          ,-.2D-13                    ,
     K     -.0D-13                          , .4D-13                    ,
     L      .11D-12                         , .11D-12                   ,
     M     -.14D-12                         ,-.75D-12                   ,
     N     -.145D-11                        ,-.108D-11                  ,
     O      .279D-11                        ,.1318D-10                  ,
     P      .3067D-10                       , .4513D-10                 ,
     Q      .1645D-10                       ,-.17396D-9                 ,
     R     -.87079D-9                       ,-.321153D-8                ,
     S     -.1180972D-7                     ,-.5028543D-7               ,
     T     -.27296205D-6                    ,-.20039404D-5              ,
     U     -.2119852312D-4                  ,-.3728518201D-3            ,
     V     -.1876272514D-1                  , .7971427704844D0          /
      REAL*8 VK1,VI1,X,Y,Z,Q1,Q2,Q3,FX,X1,X2,X3,X4,XD
      REAL * 8 XLG/Z7FFFFFFFFFFFFFFFF/
      EQUIVALENCE(A(19),B(1)),(B(19),C(1))
      IENT=1
      X=DBLE(S)
      GO TO 44
      ENTRY FF04AD(VI1,VK1,XD,N)
      IENT=2
      X=XD
   44 Y=DABS(X)
      Z=Y*.125D0
      IF(Z .GT.1D0)GO TO 42
      IF(Z .LE. 0D0)GO TO 78
      X2=4D0*Z*Z-2D0
      JUMP=1
      N1=1
      N2=18
   70 Q3=0D0
      Q2=0D0
      DO 40 I=N1,N2
      Q1=Q2
      Q2=Q3
   40 Q3=X2*Q2-Q1+A(I)
      FX=(Q3-Q1)*.5D0
      GO TO(50,51,52,53),JUMP
   50 VI1=FX*Z
      IF(IENT.EQ.1)VIS=SNGL(VI1)
      IF(N.LE.0)GO TO 75
      JUMP=2
```

```
      N1=19
      N2=56
      GO TO 70
   78 VK1=XLG
      VI1=0D0
      IF(IENT .EQ. 2)GO TO 75
      VKS=XLG
      VIS=0.
      GO TO 75
   51 VK1=VI1+DLOG(Z)+1D0/Y-Z+FX
      IF(IENT.EQ.1)VKS=SNGL(VK1)
   75 RETURN
   42 Z=1D0/Z
      X2=7+Z

      JUMP=3
      N1=57
      N2=62
      X1=1D0/DSQRT(Y)
      X3=DEXP(Y)
      IF(N-1)70,100,70
   52 VI1=X3*FX*X1
      IF(IENT.EQ.1)VIS=SNGL(VI1)
  100 IF(N.EQ.0)GO TO 75
  101 JUMP=4
      X2=-7-Z
      GO TO 70
   53 VK1=3.14159265358979300*X1*FX/X3
      IF(IENT.EQ.1)VKS=SNGL(VK1)
      GO TO 75
      END
```

LIST OF REFERENCES

1. Brunauer, S., Emmett, P. H., and Teller, E., J. Am. Soc., 60, 309 (1938).

2. Nelsen, F. M., and Eggertsen, F. T., Analytical Chemistry, 30, 1387 (1958).

3. Walker, Jr., R. D., Seventeenth Semi-Annual Report, May, 1974, NASA Research Grant NGR 10-005-022.

4. Giner, J., and Hunter, C., J. Electrochem. Soc., 116, 1124 (1969).

5. Austin, L. G., and Almaula, S., J. Electrochem. Soc., 114, 927 (1967).

6. Kordesch, K. V., From Electrocatalysis to Fuel Cells, Washington: Washington University Press (1972), p. 157.

7. Miller, M. L., and Fornasar, H. J., J. Electrochem. Soc., 115, 330 (1968).

8. Lundquist, J. T., and Vogel, W. M., J. Electrochem. Soc., 116, 1066 (1969).

9. Bockris, J. O'M., Modern Electrochemistry, New York: Plenum Press (1970), pp. 117-134.

10. Bockris, J. O'M., and Saluja, P. P. S., J. Phys. Chem., 76, 2140 (1972).

11. Hirshfelder, J. O., Curtiss, C. F., and Bird, R. B., Molecular Theory of Gases and Liquids, New York: John Wiley & Sons, Inc. (1954), p. 718.

12. Merenkov, P. T., Uzbeksh Khim. Zn., 9, 50 (1961).

13. Knobel, N., et al., J. Am. Chem. Soc., 45, 77 (1923).

14. Bhatia, R. N., M. S. Thesis, University of Florida, Gainesville, Florida (1967).

15. Perry, J. H., Chemical Engineer's Handbook, 4th Ed., 3-77 (1963).

16. Evans, U. R., Nature, 218, 602 (1968).

17. Goldstein, J. R., and Tseung, A. C. C., Nature, 222, 869, (1969).

18. Gnanamuthu, D. S., and Petrocelli, J. V., J. Electrochem. Soc., 114, 1036 (1967).

19. Newman, J. S., Electrochemical Systems, New Jersey; Prentice Hall (1973), p. 243.

20. Newman, J. S., Electrochemical Systems, New Jersey; Prentice Hall (1973), p. 245.

21. Tham, M. K., Private communication (1976).

22. Klochko, M. A., and Godneva, M. M., Russ. J. Inorg. Chem., 4, 964 (1959).

23. Bockris, J. O'M., and Srinivasan, S., Fuel Cells: Their Electrochemistry, New York: McGraw-Hill (1969), p. 289.

24. Zeliger, H. I., J. Electrochem. Soc., 113, 236 (1966).

25. Zeliger, H. I., Ibid., 114, 144 (1967).

26. Bird, R. B., Stewart, W. E., and Lightfoot, E. N., Transport Phenomena, New York: John Wiley & Sons, Inc. (1969), p. 559.

BIOGRAPHICAL SKETCH

Myung-Cheen Lee was born on December 25, 1942, in Seoul, Korea. He graduated from Kyunggi High School in Seoul, Korea in March, 1961, and received the degree of Bachelor of Science in Engineering from the Seoul National University in February, 1965.

After serving two years in the Army of the Republic of Korea, he worked with Korea Explosives Company in Seoul, Korea until beginning graduate studies at the University of Florida in September, 1971. He received the degree of Master of Engineering in chemical engineering from the University of Florida in August, 1973. He is married to Jungboon Yoon and has one child.

I certify that I have read this study and that in my opinion it conforms to acceptable standards of scholarly presentation and is fully adequate, in scope and quality, as a dissertation for the degree of Doctor of Philosophy.

Robert D. Walker, Jr., Chairman
Professor of Chemical Engineering

I certify that I have read this study and that in my opinion it conforms to acceptable standards of scholarly presentation and is fully adequate, in scope and quality, as a dissertation for the degree of Doctor of Philosophy.

Dinesh O. Shah
Professor of Chemical Engineering

I certify that I have read this study and that in my opinion it conforms to acceptable standards of scholarly presentation and is fully adequate, in scope and quality, as a dissertation for the degree of Doctor of Philosophy.

Herbert E. Schweyer
Professor of Chemical Engineering

I certify that I have read this study and that in my opinion it conforms to acceptable standards of scholarly presentation and is fully adequate, in scope and quality, as a dissertation for the degree of Doctor of Philosophy.

Charles P. Luehr
Associate Professor of Mathematics

I certify that I have read this study and that in my opinion it conforms to acceptable standards of scholarly presentation and is fully adequate, in scope and quality, as a dissertation for the degree of Doctor of Philosophy.

Antal Majthay
Associate Professor of Management

This dissertation was submitted to the Graduate Faculty of the College of Engineering and to the Graduate Council and was accepted as partial fulfillment of the requirements for the degree of Doctor of Philosophy.

December, 1976

Dean, College of Engineering

Dean, Graduate School

UNIVERSITY OF FLORIDA
3 1262 08394 246 5